NASA Contractor Report 4414

A Unified Viscous Theory of Lift and Drag of 2-D Thin Airfoils and 3-D Thin Wings

John E. Yates

PURCHASE ORDER L-74809C
DECEMBER 1991

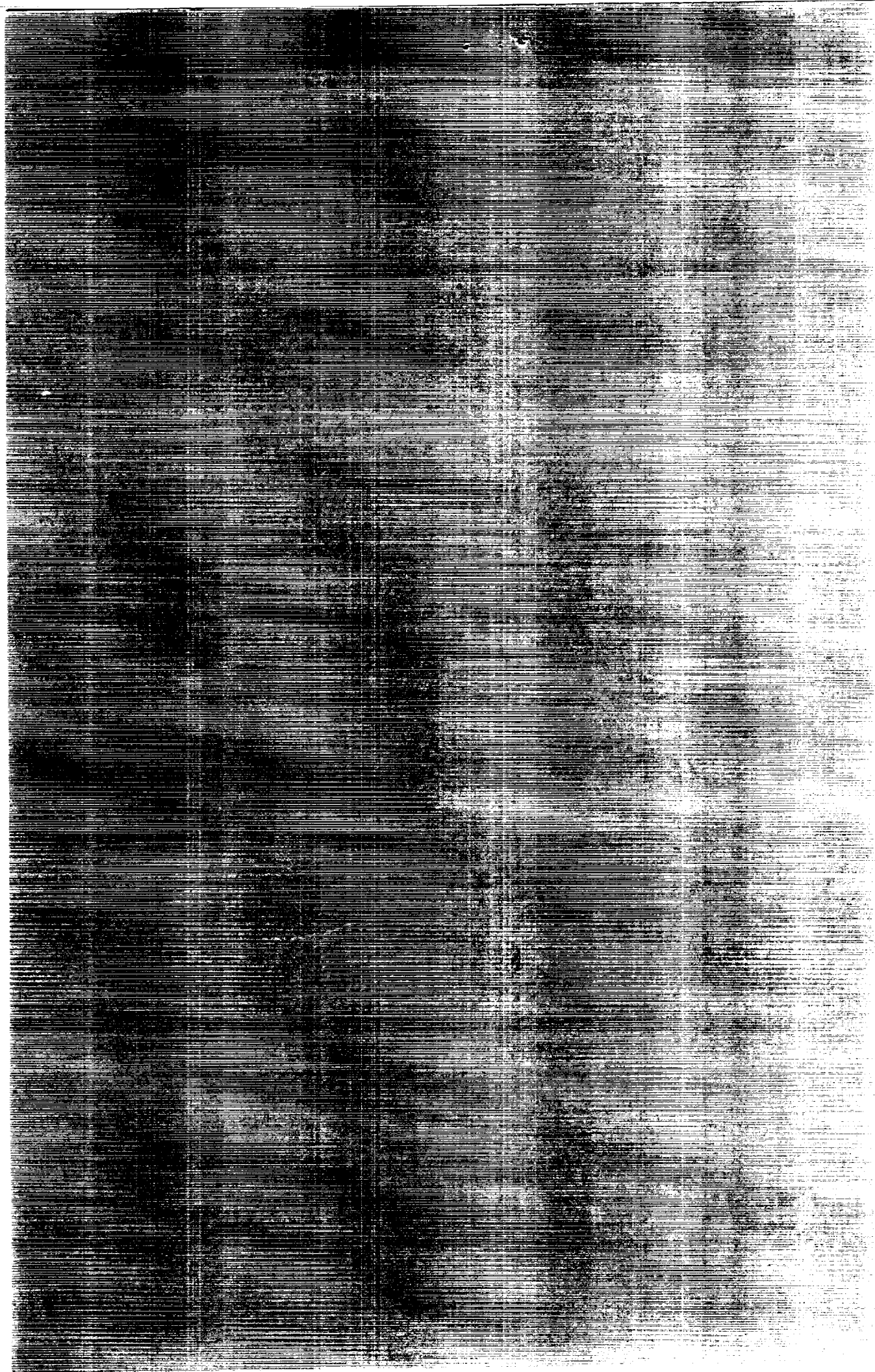

NASA Contractor Report 4414

A Unified Viscous Theory of Lift and Drag of 2-D Thin Airfoils and 3-D Thin Wings

John E. Yates
A.R.A.P. Group
California Research & Technology Division
Titan Corporation
Princeton, New Jersey

Prepared for
Langley Research Center
under Purchase Order L-74809C

National Aeronautics and
Space Administration

Office of Management

Scientific and Technical
Information Program

1991

Abstract

A unified viscous theory of 2-D thin airfoils and 3-D thin wings is developed with numerical examples. The viscous theory of the load distribution is unique and tends to the classical inviscid result with Kutta condition in the high Reynolds number limit. A new theory of 2-D section induced drag is introduced with specific applications to three cases of interest: 1) constant angle of attack; 2) parabolic camber; and 3) a flapped airfoil. The first case is also extended to a profiled leading edge foil. The well-known drag due to absence of leading edge suction is derived from the viscous theory. It is independent of Reynolds number for zero thickness and varies inversely with the square root of the Reynolds number based on the leading edge radius for profiled sections. The role of turbulence in the section induced drag problem is discussed. A theory of minimum section induced drag is derived and applied. For low Reynolds number the minimum drag load tends to the constant angle of attack solution and for high Reynolds number to an approximation of the parabolic camber solution. The parabolic camber section induced drag is about 4 percent greater than the ideal minimum at high Reynolds number. Two new concepts, the viscous induced drag angle and the viscous induced separation potential are introduced. The separation potential is calculated for three 2-D cases and for a 3-D rectangular wing. The potential is calculated with input from a standard doublet lattice wing code without recourse to any boundary layer calculations. Separation is indicated in regions where it is observed experimentally. The classical induced drag is recovered in the 3-D high Reynolds number limit with an additional contribution that is Reynolds number dependent. The 3-D viscous theory of minimum induced drag yields an equation for the optimal spanwise and chordwise load distribution. The design of optimal wing tip planforms and camber distributions is possible with the viscous 3-D wing theory.

Table of Contents

List of Figures

NOTATION

A	aspect ratio, b^2/S
a, a_{exp}	profiled airfoil drag parameter, see (2.2.55–57)
B	vorticity stream function, see (3.1.8)
b	wing span
c	2-D airfoil chord or mean aerodynamic chord
c_D, C_D	drag-due-to-lift coefficient (2-D, 3-D)
$c_{D_{min}}$	minimum section drag coefficient
c_L, C_L	lift coefficients (2-D & 3-D)
D_{turb}	drag due to turbulent enstrophy, see (2.2.58)
$\tilde{E}$	see (2.2.39)
$E_1(z)$	exponential integral, see (3.1.26)
$F(x), F(x,y)$	universal minimum drag load, see (2.2.32) or (3.1.31)
$f(x), f(x,y)$	camber shape
$H(x)$	Heaviside step function
K, E	elliptic integrals of the first and second kind
K_0	modified Bessel function
K_D	section induced drag kernel function, see (2.1.35) and Figure 2-3 or (3.1.32) and Figure 3-2
K_E	viscous part of the 3-D induced drag kernel, see (3.1.24)
K_L	load kernel function, see (2.1.16) on Figure 2-2 or (3.1.20) and Figure 3-11.
K_v	3-D kernel for separation potential, see (3.1.37) and (3.2.3).
$\ell(x), \ell(x,y)$	load distributions
L	lift
$L(y)$	span load distribution
r_N	nose radius of profiled airfoil
p	pressure
q_0, q_1	source strengths
R	Euclidean distance between two points
Re	Reynolds number — ref chord
R_N	Reynolds number — ref nose radius

S	planform area
T	Trefftz plane
u,v,w	Cartesian velocity component
U_∞	free stream velocity
V	volume of all space
(x,y,z) or (ξ,η,ζ)	Cartesian coordinates
$x_0(y)$, $x_e(y)$	wing leading and trailing edges
$\alpha,\alpha(x)$, $\alpha(x,y)$	angle of attack, negative slope of the camber shape
α_d	viscous induced drag angle, see (2.1.31)
α_v	separation potential, see (2.1.48) or (3.2.4), also Figure 2-12 and Figure 3-3.
$\delta(x)$	delta function
$\Delta\varphi$	doublet strength, see (3.1.39) or (3.3.19)
$\Delta\varphi_e$	wake doublet strength or section load (3.3.44)
Γ	total circulation
γ	circulation/unit length
γ_x,γ_y	3-D circulation components, see (3.2.6)
μ,υ	dynamic and kinematic viscosity
ρ	density
σ	Reynolds number — ref quarter chord
ω	vorticity
∇^2	Laplace operator
$\|\ \|$	denotes absolute value
$\|F\|$	integral of F over chord or planform
$(\vec{q})$	vector quantity q

I. Introduction

The work reported herein is a direct outgrowth of two previous studies, Yates (1980), and Yates and Donaldson (1986). The earlier work on 2-D viscous thin airfoil theory (also see Yates 1982 for 3-D wing results) focused on the direct role of viscosity in the generation of lift. The direct effect of the primary viscous boundary layer was taken out of the lift problem by considering the surface to move tangentially at the speed calculated with potential theory in its non-lifting attitude—the so-called "*belt sander*" model. We use this concept throughout the present study. When the airfoil is placed at a small angle of attack, the perturbation viscous boundary conditions induce an interactive vorticity field due to the surface pressure gradients. This field of local vorticity is responsible for the lift via the integral relation

$$L = \rho U_\infty \int_S \omega \, dxdy \tag{1.1}$$

where S is the 2-D region of flow outside the foil. The complete theory of the 2-D foil including finite thickness and unsteady motion was documented in Yates (1980). A very important feature of the viscous wing theory is that the load distribution is uniquely determined without recourse to the empirical Kutta condition. Furthermore, the lift is established by the action of viscosity over the entire wetted surface and not merely the local region near the trailing edge. In this early study we calculated the lift as a function of Reynolds number. For $Re \to \infty$, the lift tends to the Kutta Joukowski value

$$c_L = 2\pi\alpha \tag{1.2}$$

in accordance with earlier results of Shen and Crimi (1965) with corrections of order $(1\sqrt{\mathrm{Re}})$. Further calculations for finite trailing edge thickness indicate a proportional reduction of the lift. These and many other results were documented in our earlier work.

The effort summarized in Yates and Donaldson (1986) was concerned primarily with the problem of drag-due-to-lift. An attempt was made to rationally assess various proposed and functioning devices for reducing this important drag component. To provide a consistent framework for this task, we revisited the theoretical foundations of the theory of drag. Many known representations for the drag were rederived using the momentum integral approach. By definition the drag can be expressed as the resultant of pressure and

viscous forces on the surface or as a momentum flux integral in the Trefftz plane—all well-known results. The difficulty with using either of these formulas to attack the drag assessment problem is that two many flow variables are involved (velocity, pressure viscous stress, etc.). At the insistence of Donaldson, an all out effort was made to express the drag in terms of a single flow property. The trick for achieving this goal was to introduce the energy equation into the Trefftz plane momentum representation of the drag and then allow the Trefftz plane to recede to downstream infinity. This leads to a relationship for the power, U_∞ times the Drag, as the total viscous dissipation in the fluid as required by thermodynamics. The crucial step was to show that in an incompressible fluid the total dissipation can be rewritten as the global enstrophy or that

$$D = \frac{\mu}{U_\infty} \int_V |\vec{\omega}|^2 dV \tag{1.3}$$

where μ is the viscosity and $\vec{\omega}$ is the vorticity. This is an exact relation that contains all components of drag by whatever engineering name we may give them. Since the lift can also be expressed entirely in terms of vorticity,

$$L = \rho U_\infty \int_T dS\, \omega_x \cdot y, \tag{1.4}$$

where ω_x is the streamwise component of vorticity and T is the Trefftz plane, we have all components of the resultant force expressed in terms of vorticity alone. Many of the results in Yates and Donaldson (1986) are a direct result of these important formulas. The experimentally verified universal nature of the drag polar (e.g., see Rooney 1990) follows at once from the respective linear and quadratic dependence of the lift and drag on vorticity. Also, to the Authors knowledge, the dissipation or enstrophy formula for the drag is the only form that shows unequivocally that the drag is positive or in the direction of the external steady flow.

During the course of the 1986 effort, the Author wrote a technical memorandum that outlined the development of a unified viscous approach to the theory of lift and drag (Yates 1986). The above formulas (1.3) and (1.4) together with the earlier work on viscous airfoil theory formed the core of the idea. We had seen that lift could be expressed entirely in terms of the interactive vorticity without reference to the vorticity in the primary

boundary layer – removed with the "*belt sander*" model. Even without the artifact of a moving surface we observed that the vorticity on a symmetric airfoil section at zero lift has odd parity (top to bottom) and thus integrates to zero under the spatial averaging operation (1.1). The interactive vorticity associated with the lift has even parity and yields a finite number upon integration. If we denote these two components symbolically by $\vec{\omega}_0$ and $\vec{\omega}_1$ we can write in 3-D flow

$$\vec{\omega} = \vec{\omega}_0 + \vec{\omega}_1$$
$$|\vec{\omega}|^2 = |\vec{\omega}_0|^2 + 2\vec{\omega}_0 \cdot \vec{\omega}_1 + |\vec{\omega}_1|^2 \tag{1.5}$$

But the product of an even and odd function is odd and thus integrates to zero. Thus

$$L = \rho U_\infty \int_T ds\, \omega_x^1 y$$

and

$$D = \frac{\mu}{U_\infty}\int_V |\vec{\omega}_0|^2 dV + \frac{\mu}{U_\infty}\int_V |\vec{\omega}_1|^2 dV \tag{1.6}$$

The drag-due-to-lift is given by the second integral in (1.6). The idea that evolved was to use the interactive vorticity that we computed with the linear viscous theory in the quadratic expression for the drag, and thereby calculate the drag-due-to-lift from first principles. That is the primary subject of the present report.

In Section II, we develop the basic viscous theory of the thin 2-D airfoil and present a collection of asymptotic and numerical results. The calculation of section drag-due-to-lift and the minimum section drag load distribution is a significant new contribution to the subject. A detailed derivation of the section drag of a flat plate at angle of attack is given–a Reynolds number independent result that agrees with experiment. Also, a composite formula for the Reynolds dependent drag of a profiled section is suggested and compared with experimental data. Also, we introduce the concept of a viscous separation potential in Section II that follows from an expanded interpretation of our earlier viscous theory of lift. Preliminary examples indicate that this function could become a valuable design tool.

In Section III, we develop the viscous theory for the 3-D wing with asymptotic and numerical results. The Reynolds dependent formula for drag-due-to-lift contains the

classical induced drag as well as the section drag-due-to-chordwise load variations of the 2-D theory. The corresponding theory of minimum drag yields an integral equation for the optimal chordwise and spanwise load distribution. The theory of the 3-D separation potential for high Reynolds number deserves further development and application. A preliminary example for the rectangular wing indicates a large potential for separation at the wing tips as we might expect. Also, the theory indicates that more pointed wing tips have a considerably reduced potential for separation.

In conclusion, we remark that many of the results in this report were first outlined at an AIAA sponsored workshop on drag in which the Author participated as an invited lecturer (Yates 1990), under NASA Langley sponsorship. The AIAA notes should be used in conjunction with the present document. The author found that considerable scientific interest has been generated in the formula for drag (1.3). J. van der Vooren and J.W. Slooff presented work on the compressible counterpart of our 1986 formula while J.D. McLean presented detailed calculations of viscous drag that used the formula directly with input provided by boundary layer theory (see AIAA Professional Studies Series 1990). Earlier work of Greene (1988) on viscous induced drag was also discussed by Yates in the AIAA notes. A recent comprehensive discussion of many aspects of the compressible viscous theory may be found in Horne et al. (1990). This important work was provided to the author by Horne just prior to the AIAA drag workshop but was not included in the reference list.

II. Complete Viscous Theory of the 2-D Thin Airfoil

2.1 Basic viscous theory

The complete viscous theory of the two-dimensional zero-thickness airfoil is developed in detail. The theory is *complete* in the sense of Birkhoff's reversibility paradox:

> *Any reversible (inviscid) theory of fluid dynamics is either incomplete, over determined or grossly incorrect, so far as its prediction of steady state lift and drag are concerned.*
>
> Birkhoff (1955)

By including viscosity at the outset we obtain a well posed problem for lift and drag that does not require auxiliary empirical conditions as does the inviscid theory. The theory of lift follows closely the earlier work of Yates (1980). The complete and powerful theory of section induced drag grew out of a study of Yates and Donaldson (1986). Part of this work was included in a course on drag and lift for the AIAA (see Yates 1990). The theory of the separation potential is completely new to the author's knowledge. For completeness, we develop the 2-D theory from scratch herein even though the theory of lift was first derived over a decade ago. Many of the ideas of the lift theory can be brought into much sharper focus when considered along with the drag problem.

Consider a 2-D zero thickness airfoil of chord c fixed in a steady viscous incompressible flow (U_∞, ρ) along the x-axis. We scale all lengths by the semi-chord $c/2$, all velocities by U_∞ and pressure by ρU_∞^2. The natural Reynolds number of the problem is referred to the quarter chord:

$$\sigma = \frac{U_\infty c}{4\upsilon} \tag{2.1.1}$$

where υ is the kinematic viscosity. The problem is illustrated in Figure 2-1.

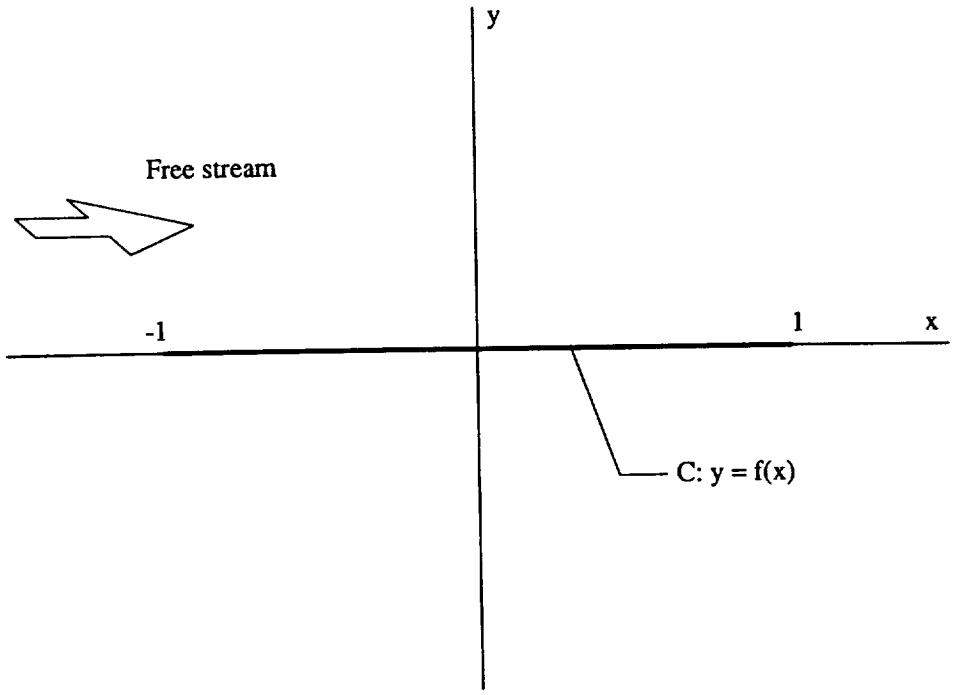

Figure 2-1. The 2-D airfoil problem.

The present theory is concerned solely with the prediction of lift and drag due to small perturbations $y = f(x)$ of the surface $C : y = 0 \pm; |x| < 1$. Following Yates (1980) we use a "*belt sander*" model to remove the mean boundary layer on C. Suppose that the upper and lower surfaces of C move at the free stream velocity. Then the exact viscous solution of the flow past C is the trivial potential flow solution. When we perturb C to the state $y = f(x)$, the viscous problem for the perturbation velocity, pressure and vorticity becomes,

$$\begin{aligned}
\frac{\partial u}{\partial x} + \frac{\partial v}{\partial y} &= 0 \\
\frac{\partial p}{\partial x} + \frac{\partial u}{\partial x} &= -\frac{1}{2\sigma}\frac{\partial \omega}{\partial y} \\
\frac{\partial p}{\partial y} + \frac{\partial v}{\partial x} &= \frac{1}{2\sigma}\frac{\partial \omega}{\partial x} \\
\omega &= \frac{\partial v}{\partial x} - \frac{\partial u}{\partial y}
\end{aligned} \qquad (2.1.2)$$

with the viscous boundary conditions

$$u = 0 \quad \text{and} \quad v = f'(x) = -\alpha(x) \quad \text{on} \quad y = 0\pm \tag{2.1.3}$$

The homogeneous no-slip condition on the perturbation velocity follows from the use of the belt sander model and distinguishes the present theory from the conventional Oseen model (Shen and Crimi 1965, also Southwell and Squire 1933). By cross differentiating the momentum equations in (2.1.2) we obtain a useful alternative formulation in terms of pressure and vorticity:

$$\begin{aligned} \nabla^2 p &= 0 \\ \frac{\partial \omega}{\partial x} &= \frac{1}{2\sigma}\nabla^2 \omega \end{aligned} \tag{2.1.4}$$

with the boundary conditions

$$\begin{aligned} \frac{\partial p}{\partial x} &= -\frac{1}{2\sigma}\frac{\partial \omega}{\partial y} \\ f''(x) + \frac{\partial p}{\partial y} &= \frac{1}{2\sigma}\frac{\partial \omega}{\partial x} \quad \text{on} \quad y = 0\pm \end{aligned} \tag{2.1.5}$$

These are the physical boundary conditions that relate the production of the linear interactive vorticity to gradients of the pressure that are driven by the geometric disturbance *f(x)*. The vorticity formulation of the problem is fundamental since the lift and drag due to the camber disturbance *f(x)* can both be expressed in terms of ω; i.e.,

$$\begin{aligned} c_L &= \frac{L}{\frac{1}{2}\rho U_\infty^2 c} = -\iint_{-\infty} \omega \, dxdy \\ c_D &= \frac{D}{\frac{1}{2}\rho U_\infty^2 c} = \frac{1}{2\sigma}\iint_{-\infty} \omega^2 \, dxdy \end{aligned} \tag{2.1.6}$$

The above relations are exact as are the linear boundary conditions (2.1.5). The lift is proportional to the total vorticity or circulation that the foil can store—hence our interpretation that an airfoil is a vorticity capacitor (Yates 1990). The drag is the global integral of the square of the vorticity divided by the Reynolds number. For the present linear problem this exact result yields the section drag-due-to-lift. The profile drag has

been removed via the belt sander model. Our claim to completeness of the present theory follows directly from this elegant positive definite representation of the drag in terms of ω.

Integral representations

The viscous perturbation problem can be recast as a problem for the single load function

$$\ell(x) = p(x,0^-) - p(x,0^+) \tag{2.1.7}$$

The procedure is to use integral representations for p and ω that follow from the fundamental solutions of (2.1.4). We have

$$p = \frac{\partial}{\partial y}\int_{-1}^{1} d\xi\, q_0(\xi)\ell n\, R$$

$$\omega = \frac{\partial}{\partial x}\int_{-1}^{1} d\xi\, q_1(\xi)e^{\sigma(x-\xi)}K_0(\sigma R) \tag{2.1.8}$$

with

$$R = [(x-\xi)^2 + y^2]^{1/2} \tag{2.1.9}$$

where q_0, q_1 are unknown distributions and K_0 is the modified Bessel function (Abramowitz and Stegun 1964). The representation of the velocity components (u,v) follows from the momentum equations in (2.1.2) with the assumption that u,v vanish far upstream. Thus

$$u = -p - \frac{1}{2\sigma}\int_{-\infty}^{x} dx \frac{\partial \omega}{\partial y}$$

$$v = -\int_{-\infty}^{x} dx \frac{\partial p}{\partial y} + \frac{\omega}{2\sigma} \tag{2.1.10}$$

or with (2.1.8)

$$u = -\frac{\partial}{\partial y}\int_{-1}^{1} d\xi\; q_0(\xi)\ell n\, R - \frac{1}{2\sigma}\frac{\partial}{\partial y}\int_{-1}^{1} d\xi\; q_1(\xi)e^{\sigma(x-\xi)}K_0(\sigma R)$$

$$\mathrm{v} = \frac{\partial}{\partial x}\int_{-1}^{1} d\xi\; q_0(\xi)\ell n\, R + \frac{1}{2\sigma}\frac{\partial}{\partial x}\int_{-1}^{1} d\xi\; q_1(\xi)e^{\sigma(x-\xi)}K_0(\sigma R) \qquad (2.1.11)$$

Now compute the limit of u,v for $y \to 0\pm$ and use the boundary conditions (2.1.3)

$$\begin{aligned} \lim_{y\to 0\pm} u &= \mp\pi q_0(x) \pm \frac{\pi}{2\sigma} q_1(x) = 0 \\ &\Rightarrow q_1(x) = 2\sigma q_0(x) \end{aligned} \qquad (2.1.12)$$

Also,

$$\lim_{y\to 0\pm} \mathrm{v} = \frac{\partial}{\partial x}\int_{-1}^{1} d\xi\; q_0(\xi)\Big[\ell n|x-\xi| + e^{\sigma(x-\xi)}K_0\big(\sigma|x-\xi|\big)\Big] = f'(x) \qquad (2.1.13)$$

Finally, take the limit of p as $y \to 0\pm$ and use (2.1.7) to get

$$\lim_{y\to 0\pm} p = \pm\pi q_0(x) \Rightarrow q_0(x) = -\frac{\ell(x)}{2\pi} \qquad (2.1.14)$$

Thus, we obtain an integral equation for the load function,

$$\frac{1}{2\pi}\int_{-1}^{1} d\xi\; \ell(\xi)K_L(x-\xi) = \alpha(x) = -f'(x) \qquad (2.1.15)$$

with

$$K_L(x) = \frac{\partial}{\partial x}\Big[\ell n|x| + e^{\sigma x}K_0\big(\sigma|x|\big)\Big] \qquad (2.1.16)$$

The last result may be found in Yates (1980). The kernel function K_L of the load equation is an essential element of the viscous theory. It is plotted in Figure 2-2 versus the Reynolds scale $X = \sigma x$ and compared with the Cauchy singular inviscid result. No matter

how large the Reynolds number σ, the logarithmic singularity of K_L is retained along with a more persistent downstream influence than upstream. This behavior is the reason for uniqueness of the viscous loads problem with a tendency to non-singular trailing edge behavior of the load in the high σ limit.

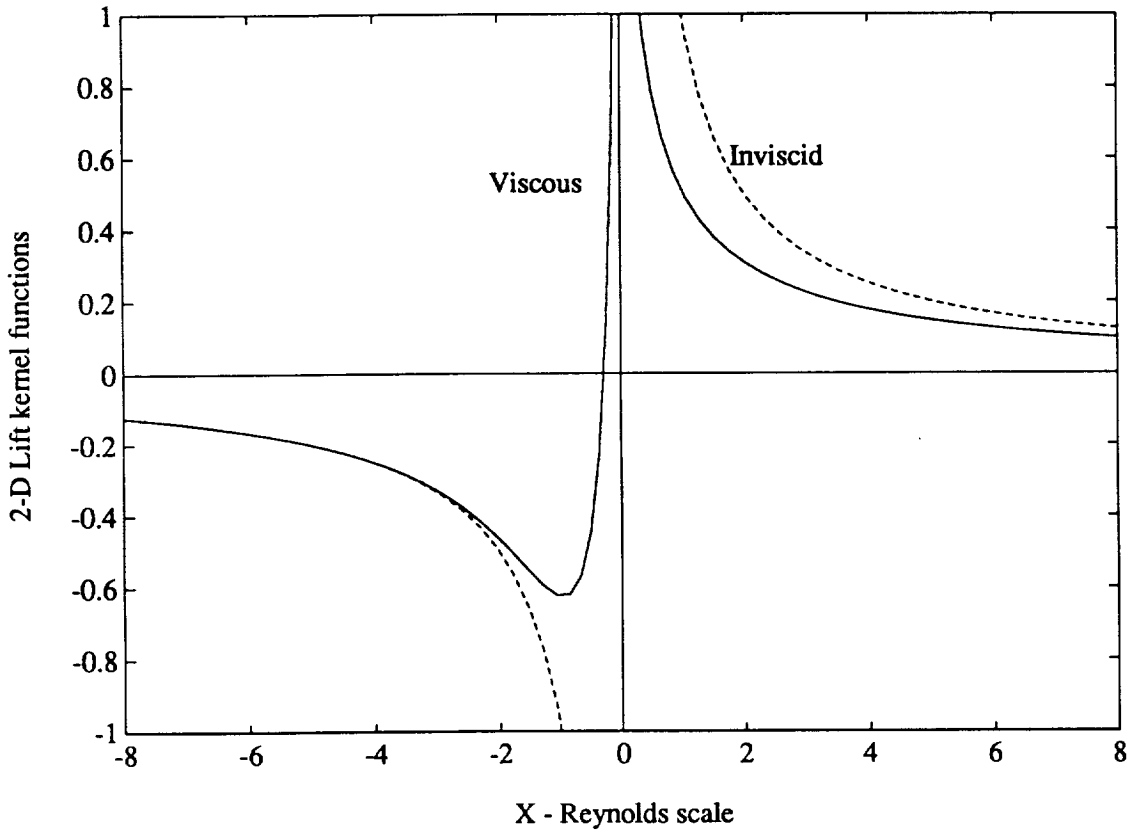

Figure 2-2. Comparison of the viscous and inviscid load kernel functions, K_L.

With the solution of (2.1.15), the velocity, pressure and vorticity are given by the following integrals:

$$u = \frac{1}{2\pi}\frac{\partial}{\partial y}\int_{-1}^{1} d\xi\, \ell(\xi)\left[\ell n\, R + e^{\sigma(x-\xi)}K_0(\sigma R)\right]$$

$$v = -\frac{1}{2\pi}\frac{\partial}{\partial x}\int_{-1}^{1} d\xi\, \ell(\xi)\left[\ell n\, R + e^{\sigma(x-\xi)}K_0(\sigma R)\right]$$

$$p = -\frac{1}{2\pi}\frac{\partial}{\partial y}\int_{-1}^{1} d\xi\, \ell(\xi)\ell n\, R$$

$$\omega = -\frac{\sigma}{\pi}\frac{\partial}{\partial x}\int_{-1}^{1} d\xi\, \ell(\xi)e^{\sigma(x-\xi)}K_0(\sigma R) \qquad (2.1.17)$$

Section lift

Next we use the above formula for ω in the integral expression for the lift (2.1.6). First we derive an intermediate result for the circulation per unit length. Define

$$\gamma(x) = -\int_{-\infty}^{\infty} dy\, \omega(x,y)$$

$$= \frac{\sigma}{\pi}\frac{\partial}{\partial x}\int_{-1}^{1} d\xi\, \ell(\xi)e^{\sigma(x-\xi)}\int_{-\infty}^{\infty} dy\, K_0(\sigma R) \qquad (2.1.18)$$

or using the known integral (Erdelyi 1954)

$$\int_{-\infty}^{\infty} dy\, K_0\left(\sigma\left(x^2+y^2\right)^{1/2}\right) = \frac{\pi}{\sigma}e^{\sigma|x|} \qquad (2.1.19)$$

we obtain

$$\gamma(x) = \frac{\partial}{\partial x}\int_{-1}^{1} d\xi\, \ell(\xi)e^{\sigma(x-\xi-|x-\xi|)} \qquad (2.1.20)$$

The section lift coefficient is given by

$$c_L = -\int_{-\infty}^{\infty} \omega \, dxdy = \int_{-\infty}^{\infty} dx \, \gamma = \Gamma$$
$$= \int_{-1}^{1} dx \, \ell(x) \qquad (2.1.21)$$

We further observe with (2.1.20) that

$$\gamma(x) = 2\sigma e^{2\sigma x} \int_{-1}^{1} d\xi \, \ell(\xi) e^{-2\sigma\xi} \qquad x < -1$$
$$= 0 \qquad x > 1 \qquad (2.1.22)$$

The circulation decays exponentially on the scale of σ upstream of the leading edge and is exactly zero downstream of the trailing edge. All of the vorticity that makes up the circulation γ or the total circulation Γ is confined to the immediate neighborhood of the foil. This remarkable result is equally valid at high lift as is the general formula for lift (2.1.6). It is the viscous counterpart of the Kutta-Joukowski theorem. The ability of any foil configuration to develop lift is one and the same as its ability to store vorticity in the near field—hence our interpretation (Yates 1990) of an airfoil as a vorticity capacitor. We hasten to point out however, that the stored vorticity is continuously replenished via the steady state transport process in (2.1.4) and the production process in (2.1.5). At high angle of attack, these processes will in general become unstable with intermittent vortex shedding.

Section induced drag

The viscous formula (2.1.6) for the section induced drag is a very important new result that enables us to complete the theory of the viscous thin airfoil. With (2.1.6) and the integral representation of the vorticity (2.1.17) we can derive a useful practical formula for the section induced drag in terms of the load $\ell(x)$. We substitute (2.1.17) into (2.1.6) and carry out the integration over the infinite domain. Thus

$$c_D = \frac{\sigma}{2\pi^2} \int_{-1}^{1} d\xi \, \ell(\xi) \int_{-1}^{1} d\eta \, \ell(\eta) \cdot \chi \qquad (2.1.23)$$

with

$$\chi = \frac{\partial^2}{\partial\xi\partial\eta}\iint_{\infty} dxdy\, e^{\sigma(x-\xi+x-\eta)}K_0(\lambda R_\xi)K_0(\lambda R_\eta) \qquad (2.1.24)$$

where the subscripts (ξ,η) on $R = (x^2+y^2)^{1/2}$ means that x is to be replaced by $x-\xi$ or $x-\eta$ respectively. The integration in (2.1.24) is completed as follows.

First consider the integral

$$\vartheta = \int_{-\infty}^{\infty} dy\, K_0[\sigma(a^2+y^2)^{1/2}]K_0[\sigma(b^2+y^2)^{1/2}] \qquad (2.1.25)$$

Replace the second Bessel argument by its Fourier cosine representation (Erdelyi 1954)

$$K_0[\sigma(b^2+y^2)^{1/2}] = \int_0^{\infty} dt\, \cos yt \frac{\exp[-|b|(t^2+\sigma^2)^{1/2}]}{(t^2+\sigma^2)^{1/2}} \qquad (2.1.26)$$

then derive the Parseval relation for ϑ;

$$\begin{aligned}\vartheta &= \int_0^{\infty} dt \frac{\exp[-|b|(t^2+\sigma^2)^{1/2}]}{(t^2+\sigma^2)^{1/2}} \int_{-\infty}^{\infty} dy \cos yt K_0(\lambda(a^2+y^2)^{1/2}) \\ &= \frac{\pi}{\sigma}\int_{\sigma(|a|+|b|)}^{\infty} K_0(t)dt \end{aligned} \qquad (2.1.27)$$

Thus, the function χ can be written as

$$\chi = \frac{\partial^2}{\partial\xi\partial\eta}\int_{-\infty}^{\infty} dx\, e^{\sigma(x-\xi+x-\eta)} \cdot \frac{\pi}{\sigma}\int_{\sigma(|x-\xi|+|x-\eta|)}^{\infty} K_0(t)dt \qquad (2.1.28)$$

or integrate by parts with respect to x to get

$$\chi = \frac{\pi}{2\sigma}\frac{\partial^2}{\partial\xi\partial\eta}\int_{-\infty}^{\infty} dx\, [sgn(x-\xi)+sgn(x-\eta)]e^{\sigma(2x-\xi-\eta)}K_0\left(\sigma\left(|x-\xi|+|x-\eta|\right)\right) \qquad (2.1.29)$$

Now we observe that $\chi(\xi,\eta)$ is symmetric with respect to an interchange of (ξ,η). Thus we assume without loss of generality that $\xi > \eta$ for the moment. Then

$$\begin{aligned}
\chi = & -\frac{\pi}{\sigma}\frac{\partial^2}{\partial\xi\partial\eta}\int_{-\infty}^{\eta} dx\, e^{\sigma(2x-\xi-\eta)}K_0\big(\sigma(\xi+\eta-2x)\big) \\
& +\frac{\pi}{\sigma}\frac{\partial^2}{\partial\xi\partial\eta}\int_{\xi}^{\infty} dx\, e^{\sigma(2x-\xi-\eta)}K_0\big(\sigma(2x-\xi-\eta)\big) \\
= & \frac{\pi}{\sigma^2}\frac{\partial^2}{\partial\xi\partial\eta}\int_{\sigma|\xi-\eta|}^{\infty} dt\, K_0(t)\sinh t \\
= & \frac{\pi}{\sigma}\frac{\partial}{\partial\xi}\Big[K_0\big(\sigma|\xi-\eta|\big)\sinh\sigma(\xi-\eta)\Big] \qquad (2.1.30)
\end{aligned}$$

which is valid for all ξ and η. Finally, we use (2.1.23) with the change of notation $(\xi,\eta) \rightarrow (x,\xi)$ to obtain the final expression for the section induced drag

$$\begin{aligned}
c_D &= \int_{-1}^{1} dx\, \ell(x)\alpha_d(x) \\
\alpha_d(x) &= \frac{1}{2\pi}\int_{-1}^{1} d\xi\, \ell(\xi)\frac{\partial}{\partial x}\Big[K_0\big(\sigma|x-\xi|\big)\sinh\sigma(x-\xi)\Big] \qquad (2.1.31)
\end{aligned}$$

where we interpret $\alpha_d(x)$ as the viscous *induced drag angle*. It plays a role in the 2-D theory much like the induced angle of attack that is familiar in 3-D lifting line theory. Numerical examples of α_d are presented in Section 2.3. The section drag is obviously quadratic in the section lift and is a function of Reynolds number σ. There is no counterpart of this important result in the familiar inviscid formulation of the 2-D airfoil problem where the section drag is exactly zero. We make extensive use of this formula in the subsequent analysis.

Minimum section induced drag

With an explicit positive definite expression for the section drag-due-to-lift we can pose a variational problem for the minimum drag—a problem that is quite familiar in

3-D wing theory but heretofore non-existent in the 2-D theory. We seek a minimum of (2.1.31) with the constraint (2.1.21) on the total lift. Consider the functional

$$J[\ell] = D[\ell] - \lambda[\int_{-1}^{1} dx\, \ell - c_L] \tag{2.1.32}$$

where λ is a Lagrange multiplier. Now require J to be a minimum with respect to $\ell(x)$ and λ,

$$\delta J = 0 \quad \text{and} \quad \frac{\partial J}{\partial \lambda} = 0 \tag{2.1.33}$$

The variation of J yields the Euler equation for ℓ,

$$\frac{1}{\pi}\int_{-1}^{1} d\xi\, \ell(\xi) K_D(x-\xi) = \lambda \tag{2.1.34}$$

with

$$K_D(x) = \frac{\partial}{\partial x}\left(K_0(\sigma|x|)\sinh \sigma x\right) \tag{2.1.35}$$

The constraint on ℓ is,

$$\int_{-1}^{1} \ell(x)dx = c_L \tag{2.1.36}$$

and the minimum drag is obtained with (2.1.31) and (2.1.34),

$$c_D = \frac{c_L \lambda}{2} \tag{2.1.37}$$

Since it is redundant to retain both λ and c_L, we define the universal load function $F(x)$ with

$$\ell(x) = \frac{\lambda}{2} F(x) \tag{2.1.38}$$

Then $F(x)$ is the solution of

$$\frac{1}{2\pi} \int_{-1}^{1} d\xi \; F(\xi) K_D(x - \xi) = 1 \tag{2.1.39}$$

$$\lambda = 2c_L \Big/ \int_{-1}^{1} F(x) dx \tag{2.1.40}$$

and

$$c_D = c_L^2 \Big/ \int_{-1}^{1} F(x) dx \tag{2.1.41}$$

or

$$\frac{dc_D}{dc_L^2} = 1 \Big/ \int_{-1}^{1} F(x) dx \tag{2.1.42}$$

$$\ell(x) = c_L \cdot F(x) \Big/ \int_{-1}^{1} F(x)\, dx \tag{2.1.43}$$

An immediate result is evident if we compare the equation (2.1.39) for the minimum drag load with the induced drag angle in (2.1.31). The condition for minimum section drag is that the viscous induced drag angle be constant over the chord. Recall that this is also the condition for a minimum of the classical 3-D wing induced drag. The uniqueness of solution of the minimum drag equation (2.1.39) follows from the logarithmic behavior of the drag kernel K_D near the origin. This kernel is plotted versus the Reynolds scale $X = \sigma x$ in Figure 2-3.

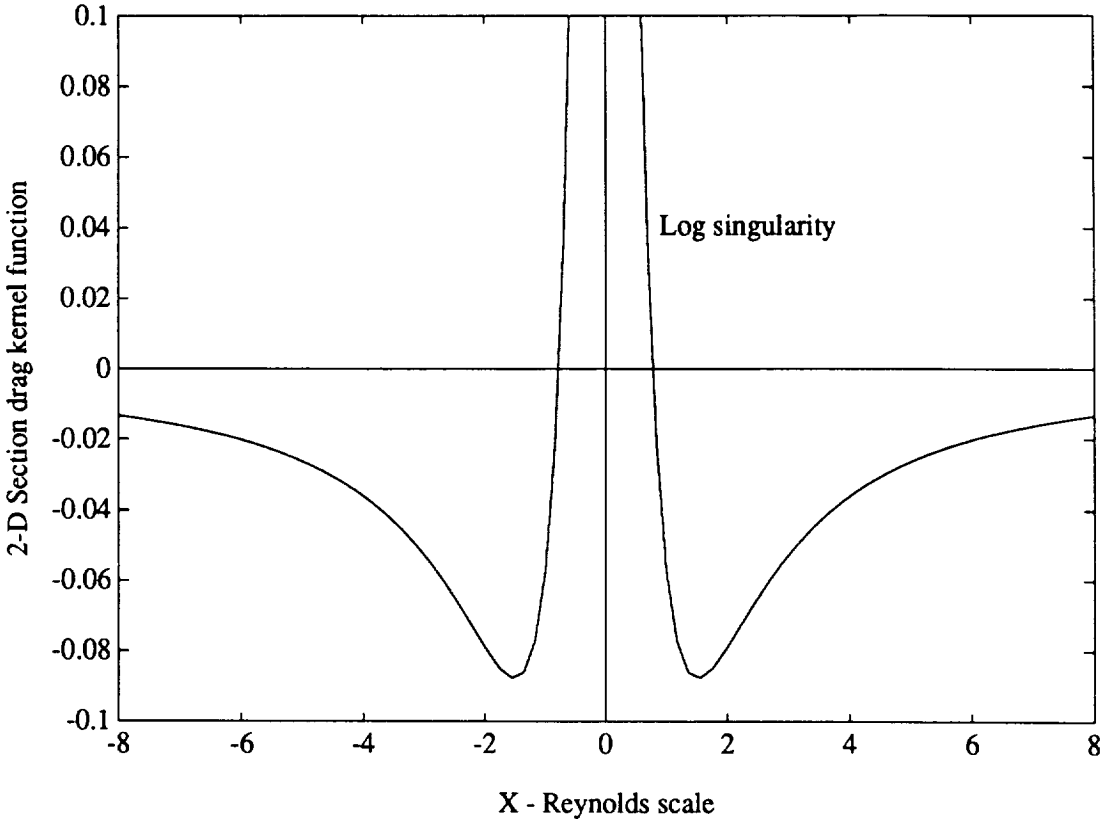

Figure 2-3. Section induced drag kernel, K_D.

The camber shape and local angle of attack that produce the minimum drag load distribution are obtained with (2.1.15),

$$f(x) = -\frac{c_L}{2\pi}\int_{-1}^{1} d\xi G(\xi)\left[\ell n|x-\xi| + e^{\sigma(x-\xi)}K_0\left(\sigma|x-\xi|\right)\right] \tag{2.1.44}$$

with

$$G(x) = F(x) / \int_{-1}^{1} F(x)\,dx \tag{2.1.45}$$

and

$$\alpha(x) = -\frac{df}{dx} \tag{2.1.46}$$

The theory of minimum induced section drag has become a theory of the optimal load distribution. Our original viscous theory of the load distribution has become a theory of the

optimal camber shape. Recall that the classical theory of minimum induced drag of 3-D wings does not provide any information about the chordwise load distribution or shape. The above analysis is an important step in the direction of a true 3-D wing design code. Detailed calculations are presented in Section 2.3.

The separation potential

Since we have removed the primary boundary layer from the formulation of the viscous perturbation problem, it may seem pointless to discuss separation. However, the theory of the load function in (2.1.15) and (2.1.16) suggests an interesting approach to the problem. We write (2.1.15) in the form

$$\frac{1}{2\pi}\int_{-1}^{}d\xi\,\frac{\ell(\xi)}{x-\xi}=\alpha(x)+\alpha_v(x) \tag{2.1.47}$$

with

$$\alpha_v(x)=-\frac{1}{2\pi}\int_{-1}^{1}d\xi\;\ell(\xi)\frac{\partial}{\partial x}e^{\sigma(x-\xi)}K_0\big(\sigma|x-\xi|\big) \tag{2.1.48}$$

The function $\alpha_v(x)$ is a viscous load induced angle of attack or when multiplied by the free stream velocity it is a viscous load induced blowing velocity. We suppose that the real boundary layer that we removed must respond to this velocity. We show below with several examples that α_v increases from leading edge to trailing edge where it becomes singular. For the class of load functions $\ell_0(x)$ that solve the corresponding inviscid problem

$$\frac{1}{2\pi}\int_{-1}^{1}d\xi\,\frac{\ell_0(\xi)}{x-\xi}=\alpha(x) \tag{2.1.49}$$

the least singular $\alpha_v(x)$ is obtained when ℓ_0 satisfies the Kutta condition at the trailing edge. This suggests that $\alpha_v(x)$ may be used as an indicator of the potential for separation. We explore this idea in more detail in subsequent sections.

2.2 Asymptotic analysis

In this section we examine the viscous theory more closely in the extreme limits of small and large quarter chord Reynolds number σ. The analysis is of interest for several reasons. First we will show that the theory of the load function and the minimum drag load function is unique—an essential feature of any "*complete*" theory. Second, we gain further insight into the meaning of the separation potential.

Low Reynolds number $\sigma << 1$

Consider the solution of the load equation (2.1.15) with the kernel function (2.1.16) when σ tends to zero. For $|x|$ bounded, we first expand the kernel. For $\sigma|x| << 1$, we have

$$K_L(x) = \frac{\partial}{\partial x}\left[\ell n\,|x| + e^{\sigma x} K_0(\sigma|x|)\right]$$
$$= -\sigma\left(\ell n\,|x| + \ell n\,\frac{\sigma}{2} + \gamma + 1\right) + O\left(\sigma^2 x\,\ell n\,\sigma|x|\right) \qquad (2.2.1)$$

where γ is Euler's constant ($\cong 0.5772$). The integral equation for the load becomes

$$-\frac{\sigma}{2\pi}\cdot\int_{-1}^{1} d\xi\;\ell(\xi)\left[\ell n\,|x-\xi| + \ell n\,\frac{\sigma}{2} + \gamma + 1\right] = \alpha(x) \qquad (2.2.2)$$

Within the class of load functions that admit a square root singularity at the leading and trailing edge, the last equation has a unique solution. This is a general feature of integral equations of the type (2.2.2) that have a log singular kernel function (e.g. see, Carrier, Krook and Pearson 1966). Since we know (see Fig. 2-2) that the logarithmic singularity is retained at all Reynolds numbers, we conclude that the solution of the load equation is unique for all σ. For the same reason, the solution of the minimum drag loads problem is unique.

We now demonstrate the solution of (2.2.2) for the special case of constant angle of attack. For then we can differentiate (2.2.2) to get

$$-\frac{\sigma}{2\pi}\int_{-1}^{1}\frac{\ell(\xi)}{x-\xi}=0 \tag{2.2.3}$$

which has the eigensolution

$$\ell(x)=\frac{C}{\sqrt{1-x^2}} \tag{2.2.4}$$

Then substitute $\ell(x)$ into (2.2.2) with $\alpha(x)=\alpha$ to get

$$C=\frac{2\alpha}{\sigma(\ell n\, 4/\sigma-\gamma-1)}$$

$$\ell(x)=\frac{2\alpha}{\sigma(\ell n\, 4/\sigma-\gamma-1)}\frac{1}{\sqrt{1-x^2}} \tag{2.2.5}$$

and

$$c_L=\frac{2\pi\ \ \alpha}{\sigma(\ell n\, 4/\sigma-\gamma-1)} \tag{2.2.6}$$

The slope of the lift curve in low Reynolds number Stokes flow becomes infinite; i.e.,

$$\frac{dc_L}{d\alpha}=\frac{2\pi}{\sigma(\ell n\, 4/\sigma-\gamma-1)}=O\left(\frac{1}{\sigma\,\ell n\, 4/\sigma}\right) \tag{2.2.7}$$

We turn now to the minimum drag problem at low Reynolds number. First expand the drag kernel function K_D in (2.1.35) to get

$$K_D(x)=\frac{\partial}{\partial x}\left(K_0(\sigma|x|)\sinh\sigma x\right)$$

$$=-\sigma\left(\ell n|x|+\ell n\frac{\sigma}{2}+\gamma+1\right) \tag{2.2.9}$$

which is identical to the low Reynolds number approximation of (2.2.1). Thus the universal minimum drag load function becomes

$$F(x) = \frac{2}{\sigma(\ell n\, 4/\sigma - \gamma - 1)} \frac{1}{\sqrt{1-x^2}}$$

$$\ell(x) = \frac{c_L}{\pi\sqrt{1-x^2}} \tag{2.2.10}$$

and

$$\frac{dc_D}{dc_L^2} = 1 / \int_{-1}^{1} F(x)\, dx$$

$$= \frac{\sigma}{2\pi}\left(\ell n \frac{4}{\sigma} - \gamma - 1\right) \tag{2.2.11}$$

$$\alpha = \frac{c_L}{2\pi}\sigma\left(\ell n \frac{4}{\sigma} - \gamma - 1\right) \tag{2.2.12}$$

As we noted above, the minimum section drag problem has a unique solution since the kernel function $K_D(x)$ has a logarithmic singularity. The induced drag number dc_D / dc_L^2 tends to zero in the low Reynolds number limit. We will show presently that this number is a maximum for $\sigma \equiv 1$. The minimum drag camber shape is the constant angle of attack given by (2.2.12),which tends to zero as $\sigma \to 0$ for fixed c_L. This is an example of two theorems that Batchelor (1967) attributes to Helmholtz:*

1. *There cannot be more than one solution for the velocity distribution for flow in a given region with negligible inertia forces and consistent with prescribed values of the velocity vector at the boundary of the region, (including a hypothetical boundary at infinity when the fluid is of infinite extent).*

2. *Flow with negligible inertia forces has a smaller total dissipation than any other incompressible flow on the same region with the same values of the velocity vector everywhere on the boundary of the region.*

Helmholtz 1868
(see Batchelor 1967)

*This author has tried unsuccessfully to obtain an extension of the second principle to higher Reynolds number via an enstrophy principle, (see Yates 1983).

High Reynolds number, $\sigma >> 1$

The motivation and objective of the viscous theory is to obtain useful and practical results at high Reynolds number. By using the belt sander model we have formally removed any real Reynolds number associated with the primary boundary layer from the problem, (e.g., δ^* or θ), even though σ is one fourth of the usual chord Reynolds number. In the language of triple deck theory, (e.g. see Melnik (1978) or Brown & Stewartson (1970)), we have eliminated the middle deck in order to get at the inherent physics of the viscous origin of lift and section induced drag. Refinements that include Reynolds number effects of the middle deck and even geometric thickness can be considered later.

First we write (2.1.15) in the form

$$\frac{\partial}{\partial x}\frac{1}{2\pi}\int_{-1}^{1} d\xi\, \ell(\xi)\Big[\ell n|x-\xi| + e^{\sigma(x-\xi)}K_0\big(\sigma|x-\xi|\big)\Big] = \alpha(x) \qquad (2.2.13)$$

and note that the contribution of the region $|x-\xi| < \lambda/\sigma$ to the integral is small when $1 << \lambda << \sigma$. Thus, we can replace the Bessel function with its asymptotic expansion; i.e.,

$$\begin{aligned} e^{\sigma x}K_0\big(\sigma|x|\big) &\equiv \sqrt{\frac{\pi}{2\sigma|x|}}e^{\sigma(x-|x|)} \\ &= \sqrt{\frac{\pi}{2\sigma x}} \qquad x > \lambda/\sigma \\ &= 0 \qquad\qquad x < \lambda/\sigma \end{aligned} \qquad (2.2.14)$$

and so for $\varepsilon = \lambda/\sigma \to 0$, we get

$$\frac{1}{2\pi}\int_{-1}^{1} d\xi \cdot \frac{\ell(\xi)}{x-\xi} + \frac{1}{2\sqrt{2\pi\sigma}}\frac{\partial}{\partial x}\cdot\int_{-1}^{1} d\xi \frac{\ell(\xi)}{\sqrt{x-\xi}} = \alpha \quad \text{for} \quad \sigma >> 1 \qquad (2.2.15)$$

where the first integral is a Cauchy principle value integral. The second term is the derivative of the Abel transform of the load. From the formulas (2.1.47) and (2.1.48) we recognize the second term as the viscous induced angle of attack; i.e.,

$$\alpha_v(x) = -\frac{1}{2\sqrt{2\pi\sigma}}\frac{\partial}{\partial x}\cdot\int_{-1}^{1} d\xi \frac{\ell(\xi)}{\sqrt{x-\xi}} \tag{2.2.16}$$

and

$$\frac{1}{2\pi}\cdot\int_{-1}^{1} d\xi \frac{\ell(\xi)}{x-\xi} = \alpha(x) + \alpha_v(x) \tag{2.2.17}$$

Constant alpha separation potential

Our first use of $\alpha_v(x)$ is to derive the asymptotic solution of (2.2.17) regarding α_v as an error term for the corresponding inviscid problem

$$\frac{1}{2\pi}\int_{-1}^{1} d\xi \frac{\ell(\xi)}{x-\xi} = \alpha \tag{2.2.18}$$

where for this example we assume α = constant. The solution of (2.2.18) is

$$\ell(x) = \frac{1}{\pi}\left(\frac{c_L - 2\pi\alpha x}{\sqrt{1-x^2}}\right) \tag{2.2.19}$$

where c_L is arbitrary. But with the viscous equation we can compute the error due to $\ell(x)$. Thus,

$$\begin{aligned}\alpha_v &= -\frac{1}{2\sqrt{2\pi\sigma}}\frac{\partial}{\partial x}\int_{-1}^{x} d\xi \frac{\ell(\xi)}{\sqrt{x-\xi}} \\ &= -\frac{1}{2\pi\sqrt{2\pi\sigma}}\cdot\frac{\partial}{\partial x}\cdot\int_{-1}^{x}\frac{d\xi}{\sqrt{x-\xi}}\left(\frac{c_L - 2\pi\alpha\xi}{\sqrt{1-\xi^2}}\right)\end{aligned} \tag{2.2.20}$$

This error angle can be evaluated explicitly (see Appendix A). We have

$$\alpha_v(x) = -\frac{1}{8\pi\sqrt{\pi\sigma}k^2}\left[(c_L - 2\pi\alpha)\left(\frac{E}{1-k^2} - K\right) + 4\pi\alpha(E-K)\right]$$

with

$$k = \sqrt{\frac{1+x}{2}} \tag{2.2.21}$$

where $E(k)$ and $K(k)$ are the standard elliptic integrals. For $x \to 1$, α_v is of order

$$\frac{1}{4\pi\sqrt{\pi\sigma}}(c_L - 2\pi\alpha)\left(\frac{\pi}{1-x}\right) \tag{2.2.22}$$

unless

$$c_L = 2\pi\alpha \tag{2.2.23}$$

in which case we obtain the much smaller logarithmic error.

$$\begin{aligned}\alpha_v(x) &= \frac{c_L}{4\pi\sqrt{\pi\sigma}}\left(\frac{K-E}{k^2}\right) \\ &= O\left(\frac{-\ell n|1-x|}{\sqrt{\sigma}}\right) \qquad \text{for} \quad x \to 1\end{aligned} \tag{2.2.24}$$

We recognize (2.2.23) as the solution of the inviscid problem with the auxiliary empirical statement of the Kutta condition. In a formal sense, we have derived the Kutta condition via the high Reynolds number viscous theory, a result first obtained by Shen and Crimi (1965) within the context of Oseen theory.

Physically, the last result is much deeper than a simple empirical statement about the nature of the trailing edge flow. In Figure 2-4, we plot the normalized separation potential $\sqrt{\sigma}\,\alpha_v / c_L$ for various values of $\frac{c_L}{2\pi\alpha}$. The reduced trailing edge singularity for $\frac{c_L}{2\pi\alpha} = 1$ is clearly evident. It is important to note the monotonic growth from the leading edge to trailing edge where it is a maximum. This is our first example of the separation potential. The response of the upper surface primary boundary layer to this viscous blowing excitation will lead to separation at some distance from the trailing edge and this distance will increase with increased angle of attack. With repeated application of

the linear viscous theory and boundary layer analysis we could in principle develop a rational theory of high lift and stall.

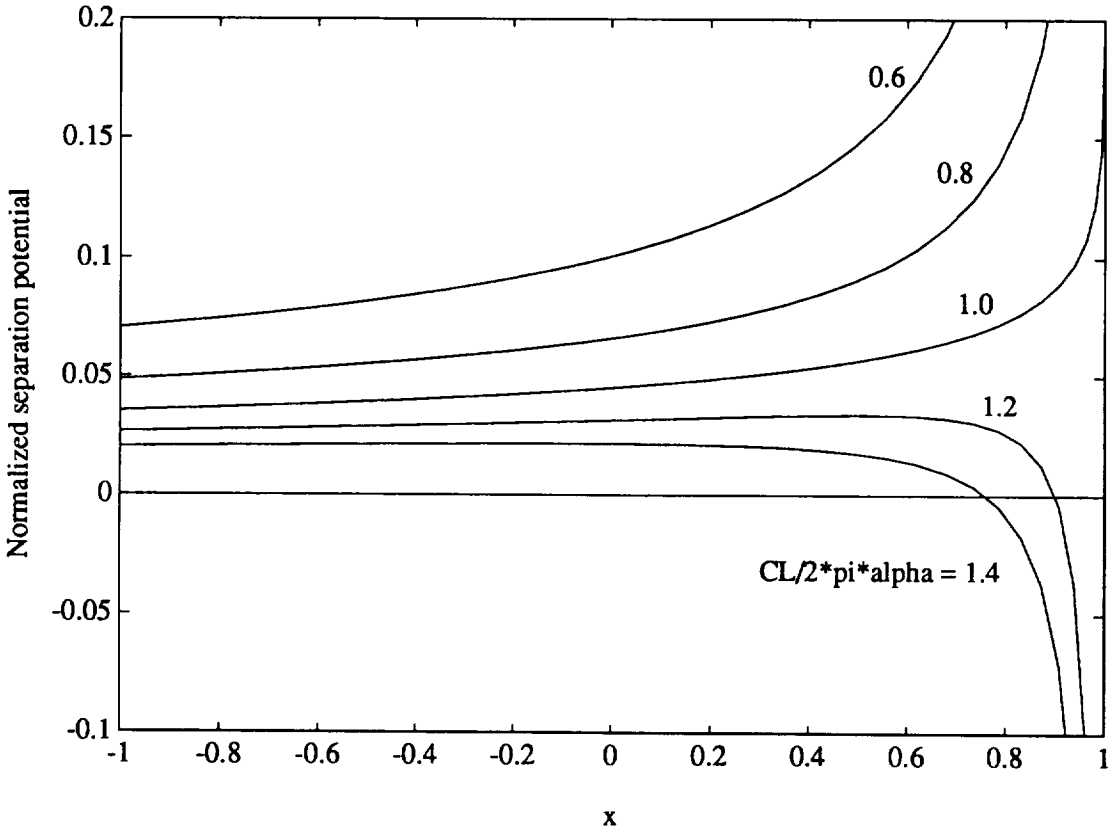

Figure 2-4. Separation potential and uniqueness of the load problem.

Parabolic camber separation potential

Another example of the separation potential is easily derived for the elliptic load distribution

$$\ell(x) = \frac{2c_L}{\pi}\sqrt{1-x^2} \tag{2.2.25}$$

and corresponding parabolic camber distribution

$$\alpha(x) = \frac{c_L}{\pi} \cdot \frac{1}{\pi} \int_{-1} d\xi \frac{\sqrt{1-\xi^2}}{x-\xi}$$

$$= \frac{c_L}{\pi} \cdot x \qquad (2.2.26)$$

The separation potential is given by

$$\alpha_v = -\frac{c_L}{\pi\sqrt{2\pi\sigma}} \frac{\partial}{\partial x} \cdot \int_{-1}^{x} \frac{d\xi\sqrt{1-\xi^2}}{\sqrt{x-\xi}} \qquad (2.2.27)$$

which again can be evaluated in terms of elliptic integrals (Appendix A). Thus for parabolic camber

$$\alpha_v(x) = \frac{c_L}{\pi\sqrt{\pi\sigma}} (K - 2E) \qquad (2.2.28)$$

which we may compare with (2.2.24) for constant angle of attack. For $x \to 1$, we have

$$\alpha_v(x) \cong \frac{c_L}{4\pi\sqrt{\pi\sigma}} K \quad \alpha = \text{constant}$$

and

$$\alpha_v(x) \cong \frac{c_L}{\pi\sqrt{\pi\sigma}} K \quad \text{parabolic camber} \qquad (2.2.29)$$

The trailing edge singularity in the parabolic camber potential is of the same logarithmic order but 4 times greater. Near the leading edge, $x \to -1$, we have

$$\begin{aligned} \alpha_v(x) &\cong c_L / 16\sqrt{\pi\sigma} && \alpha = \text{constant} \\ &\cong -c_L / 2\sqrt{\pi\sigma} && \text{parabolic camber} \end{aligned} \qquad (2.2.30)$$

We interpret the negative value of α_v as an indication of separation on the compression side of the leading edge. For the same lift coefficient and Reynolds number, the potential for separation of the parabolic cambered foil is 3 to 4 times greater than that of the foil at constant angle of attack. In Section 2.3 we consider a third example of the separation potential for the flapped airfoil which we compare with the above results. The extension of

the separation potential concept to 3-D wings in Section III has the possibility of becoming a very useful design tool.

Minimum section drag

We turn now to the high Reynolds number approximation of the minimum section induced drag problem in Section 2.1. First, we introduce the asymptotic approximation of the drag kernel given by (2.1.35),

$$K_D(x) = \frac{\partial}{\partial x} K_0(\sigma|x|)\sinh \sigma x$$
$$\equiv \frac{\partial}{\partial x}\frac{1}{2}\sqrt{\frac{\pi}{2\sigma|x|}}\,\mathrm{sgn}\,x \qquad \text{for } |x| \neq 0 \text{ and } \sigma >> 1 \tag{2.2.31}$$

Use (2.2.31) in (2.1.39) to get

$$\frac{1}{4\sqrt{2\pi\sigma}}\frac{\partial}{\partial x}\left[\int_{-1}^{x} d\xi \frac{F(\xi)}{\sqrt{x-\xi}} - \int_{x}^{1} d\xi \frac{F(\xi)}{\sqrt{\xi - x}}\right] = 1 \tag{2.2.32}$$

Now let

$$F(x) = \frac{2\sqrt{2\pi\sigma}}{\pi} G(x) \tag{2.2.33}$$

in which case G is the solution of the universal equation

$$\frac{1}{2\pi}\frac{\partial}{\partial x}\cdot\left[\int_{-1}^{x} d\xi \frac{G(\xi)}{\sqrt{x-\xi}} - \int_{x}^{1} d\xi \frac{G(\xi)}{\sqrt{\xi - x}}\right] = 1 \tag{2.2.34}$$

with the minimum section drag coefficient

$$\frac{dc_D}{dc_L^2} = \frac{1}{2}\sqrt{\frac{\pi}{2\sigma}} \Big/ \int_{-1}^{1} G(x)dx \tag{2.2.35}$$

and the minimum drag load function

$$\ell(x) = c_L\, G(x) \Big/ \int_{-1}^{1} G(x)dx \tag{2.2.36}$$

and the Reynolds number independent camber shape

$$f(x) = -\frac{c_L}{2\pi} \int_{-1}^{1} d\xi\, G(\xi) \ell n|x-\xi| \Big/ \int_{-1}^{1} G(\xi)d\xi \tag{2.2.37}$$

We compute the solution of (2.2.34) in the following section. It is evident from (2.2.35) that the minimum section induced drag is $O(1/\sqrt{\sigma})$.

Flat plate section drag

We now compute the section induced drag in the high Reynolds number limit for the flat plate foil at angle of attack. The load function is

$$\ell(x) = \frac{c_L}{\pi}\sqrt{\frac{1-x}{1+x}} \tag{2.2.38}$$

and the section drag coefficient of interest is

$$\tilde{E} = \frac{2\pi c_D}{c_L^2} = \frac{1}{\pi^2} \int_{-1}^{1} dx \sqrt{\frac{1-x}{1+x}} \int_{-1}^{1} d\xi \sqrt{\frac{1-\xi}{1+\xi}}\, K\left(\sigma|x-\xi|\right) \tag{2.2.39}$$

with

$$K(\sigma|x|) = \frac{\partial}{\partial x}\left(K_0(\sigma|x|)\sinh \sigma x\right) \tag{2.2.40}$$

and $\sigma >> 1$. First introduce the transformation

$$x = -\cos 2\theta \qquad\qquad \xi = -\cos 2\varphi \tag{2.2.41}$$

to obtain

$$\tilde{E} = \frac{16}{\pi^2} \int_0^{\pi/2} d\theta \cos^2\theta \int_0^{\pi/2} d\varphi \cos^2\varphi\, K\left(2\sigma\left|\cos^2\theta - \cos^2\varphi\right|\right) \tag{2.2.42}$$

Next rotate and stretch the coordinates $(\theta, \varphi) \rightarrow (s,t)$ with

$$\theta = \frac{s-t}{2} \qquad \varphi = \frac{s+t}{2} \tag{2.2.43}$$

Also note the symmetry in s,t to get

$$\tilde{E} = \frac{8}{\pi^2} \int_0^{\pi/2} ds \int_0^{s} dt \left(\cos^2 s + \cos^2 t\right) K(2\sigma \sin s \sin t) \tag{2.2.44}$$

Now use (2.2.40) and integrate by parts with respect to t. With the change of variables

$$\tau = 2\sigma \sin^2 s \tag{2.2.45}$$

we obtain finally

$$\begin{aligned} \tilde{E} = 1 &- \frac{4}{\pi^2} \int_{2\sigma}^{\infty} \frac{d\tau}{\tau} K_0(\tau) \sinh \tau \\ &+ \frac{4}{\pi} \int_0^{\pi/2} ds \int_0^{s} dt \frac{\left(\sin^2 s - \sin^2 t\right) \sin t}{\cos^2 t \cdot \sin s} K_0(2\sigma \sin s \sin t) \sinh(2\sigma \sin s \sin t) \end{aligned} \tag{2.2.46}$$

where we have used the definite integral,

$$\frac{4}{\pi^2} \int_0^{\infty} \frac{d\tau}{\tau} K_0(\tau) \sinh \tau = 1 \tag{2.2.47}$$

For $\sigma >> 1$, the Bessel function can be replaced with its asymptotic expansion in (2.2.46) in which case we find

$$\tilde{E} = 1 + O\left(\frac{1}{\sqrt{\sigma}}\right) \tag{2.2.48}$$

and

$$c_D = \frac{c_L^2}{2\pi} \qquad \text{for} \quad \sigma \rightarrow \infty \tag{2.2.49}$$

This is the experimentally verified result for the section induced drag of a flat plate foil (Hoerner 1965, p. 7-3). We have derived this well-known Reynolds number independent result with a complete viscous theory. The approach to this limit is calculated numerically in Section 2.3.

Profiled airfoil section drag

The present theory was derived formally for a zero thickness foil. When the Reynolds number is large the load distribution becomes identical to the classical inviscid distribution obtained with the Kutta condition and we have shown that the section drag can be obtained by tilting the resultant lift by the geometric angle of attack. Another point of view is that we have given up all "leading edge suction" a finite force that acts at the point leading edge in the limit of the classical inviscid theory as the thickness tends to zero It is natural to ask whether the present theory can yield any useful information about the nature of the leading edge suction force for a profiled leading edge. To investigate this question we consider the load function

$$\ell(x) = \frac{c_L}{2\pi} \frac{\sqrt{1-x^2}}{1+x+\varepsilon} \tag{2.2.50}$$

where ε is the foil nose radius referenced to the foil chord. This load exhibits the usual peak near the leading edge but is otherwise regular. Following the above asymptotic analysis for the zero thickness case we obtain the following expression for the section drag

$$c_D = \frac{c_L^2}{2\pi} \cdot \frac{4S}{\sqrt{2}\,\pi^{1/2}} \cdot \frac{1}{\sqrt{\sigma\varepsilon}} \tag{2.2.51}$$

with

$$T(x) = \int_0^1 d\tau \frac{\tau^2(1-\tau^4)}{\left(1+x^2(1-\tau^2)^2\right)^2\left(1+x^2(1+\tau^2)^2\right)^2}$$

$$S = \int_0^\infty dx\, x^2(1+2x^2)T(x) \cong 0.3366 \tag{2.2.52}$$

Define the Reynolds number based on the nose radius

$$R_N = \frac{U_\infty r_N}{\upsilon} = 4\frac{U_\infty c}{4\upsilon}\cdot\frac{r_N}{c} = 4\sigma\varepsilon \tag{2.2.53}$$

Then

$$\begin{aligned} c_D &= \frac{c_L^2}{2\pi}\frac{8S}{\sqrt{2}\,\pi^{3/2}}\cdot\frac{1}{\sqrt{R_N}} \\ &\cong \frac{c_L^2}{2\pi}\cdot\frac{0.342}{\sqrt{R_N}} \end{aligned} \tag{2.2.54}$$

which indicates that the section induced drag scales with the reciprocal square root of the Reynolds number based on the nose radius.

The form of (2.2.54) and the limiting form of (2.2.49) suggest the composite asymptotic relation

$$c_D = \frac{c_L^2}{2\pi}\frac{1}{1+a\sqrt{R_N}} \tag{2.2.55}$$

where the constant a is determined from (2.2.54) to be

$$a = 1/.342 \cong 3 \tag{2.2.56}$$

From data for the roughened NACA 0006, 0009 and 00012 (Abbott and von Doenhoff 1958) we infer the experimental value

$$a_{exp} \cong 0.25 \tag{2.2.57}$$

or 1/12 the theoretical value. The two composite relations are plotted in Figure 2-5. The composite section drag relation obtained with the linear viscous theory is about an order of magnitude smaller than the experimental value for practical airfoil sections. In fact it is comparable in magnitude to the section drag in the so-called laminar flow bucket (see data in Appendix IV of Abbott and von Doenhoff). The missing element of the theory is the presence of turbulent flow over the section or the turbulent enstrophy

$$D_{turb} = \frac{\mu}{U_\infty}\int\left|\vec{\omega}'\right|^2 dV \tag{2.2.58}$$

where $\vec{\omega}'$ is the turbulent component of the vorticity. The very smooth quadratic variation of the section drag with the section lift suggests that the turbulent vorticity scales directly with the section c_L so that the general form of our composite relation seems quite plausible. The parameter a simply undergoes a transition at some value of c_L or some value of R_N in Figure 2-5. The theoretical curve may be considered a lower bound on the section induced drag if laminar flow can be maintained over most of the section. This is an area of intensive current research (see Holmes 1990).

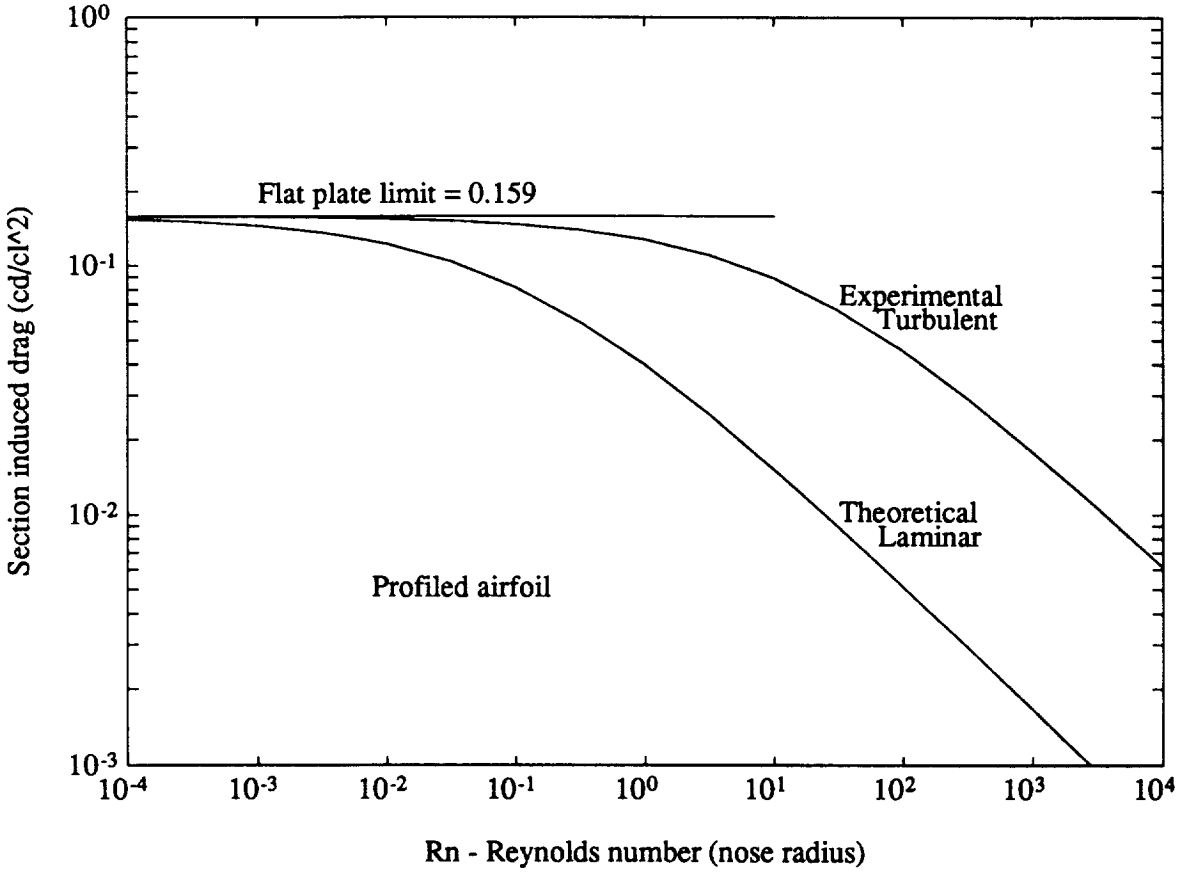

Figure 2-5. Theoretical (laminar) and experimental (turbulent) section induced drag for profiled airfoil sections.

Parabolic camber section drag

For any load distribution that is not singular at the leading edge or trailing edge the high Reynolds number section drag can be computed with (2.1.31) where we can replace the kernel with the asymptotic approximation (2.2.31). The formula is

$$c_D = \frac{1}{4\sqrt{2\pi\sigma}} \int_{-1}^{1} dx\, \ell'(x) \cdot \int_{-1}^{1} d\xi\, \ell(\xi) \frac{sgn(x-\xi)}{\sqrt{|x-\xi|}} \tag{2.2.59}$$

where the derivative $\ell'(x)$ may be singular. To illustrate this formula we compute the section drag due to the elliptic load distribution

$$\ell(x) = \frac{2c_L}{\pi} \sqrt{1-x^2} \tag{2.2.60}$$

that corresponds to parabolic camber. Break up the integral in (2.2.59) into 2 parts $x < \xi$ and $x > \xi$ and interchange the order of integration to get

$$c_D = \frac{c_L^2}{\pi^2\sqrt{2\pi\sigma}} \left\{ \int_{-1}^{1} d\xi \sqrt{1-\xi^2} \left[\int_{\xi}^{1} dx \frac{x}{\sqrt{(1-x^2)(x-\xi)}} - \int_{-1}^{\xi} dx \frac{x}{\sqrt{(1-x^2)(\xi-x)}} \right] \right. \tag{2.2.61}$$

In the first integral we let

$$\begin{aligned} x &= 1 - 2k_1^2 \sin^2\varphi \qquad 0 < \varphi < \pi/2 \\ k_1 &= \sqrt{\frac{1-\xi}{2}} \end{aligned} \tag{2.2.62}$$

and in the second integral

$$\begin{aligned} x &= 1 - 2k_2^2 \sin^2\varphi \qquad 0 < \varphi < \pi/2 \\ k_2 &= \sqrt{\frac{1+\xi}{2}} \end{aligned} \tag{2.2.63}$$

Then

$$c_D = \frac{2c_L^2}{\pi^{5/2}\sqrt{\sigma}} \int_{-1}^{1} d\xi \sqrt{1-\xi^2} \left(2E(k_1) - K(k_1)\right) \tag{2.2.64}$$

Finally set

$$\xi = \cos 2\varphi \tag{2.2.65}$$

to obtain

$$c_D = \frac{16 c_L^2}{\pi^{5/2}\sqrt{\sigma}} \int_0^{\pi/2} d\varphi \sin^2\varphi \cos^2\varphi [2E(\sin\varphi) - K(\sin\varphi)]$$

$$\equiv 0.1313\, c_L^2 / \sqrt{\sigma} \quad \text{parabolic camber} \tag{2.2.66}$$

In section 2.3 we show by numerical calculation that the ideal minimum section drag is

$$c_{D_{\min}} = 0.1268\, c_L^2 / \sqrt{\sigma} \tag{2.2.67}$$

The result for parabolic camber is only about 4 percent greater than the ideal. The load and camber distributions are compared in Section 2.3.

2.3 Numerical examples

The basic algorithm

To calculate the solution of the load equation (2.1.15), the universal minimum drag load equation (2.1.39) or its high σ asymptotic approximation (2.2.34), we are faced with the need to approximate the integral

$$C(x) = \frac{1}{2\pi} \int_{-1}^{1} d\xi\, \ell(\xi) \frac{\partial}{\partial x} F(x - \xi) \tag{2.3.1}$$

Also, $C(x)$ is needed to evaluate the section induced drag (2.1.31). The function $F(x)$ for the various cases is defined as follows:

$$
\begin{aligned}
F(x) &= \ell n|x| + e^{\sigma x} K_0(\sigma|x|) && \text{load equation (2.1.15)} \\
&= K_0(\sigma|x|)\sinh \sigma x && \text{universal load equation (2.1.39) or the section induced drag (2.1.31)} \\
&= \frac{\text{sgn x}}{\sqrt{|x|}} && \text{asymptotic universal load (2.2.34) or section drag (2.2.59)}
\end{aligned}
\tag{2.3.2}
$$

To approximate the integral for all cases we consider $\ell(x)$ to be constant over intervals x_n^- to x_n^+ where x_n is a control point for each interval. Then

$$
\begin{aligned}
C(x) &= \frac{1}{2\pi} \sum_{n=1}^{N} \int_{x_n^-}^{x_n^+} \ell_n \, d\xi \, \frac{\partial}{\partial \xi} F(x-\xi) \\
&= \frac{1}{2\pi} \sum_{n=1}^{N} \ell_n \left[F(x-x_n^-) - F(x-x_n^+) \right]
\end{aligned}
\tag{2.3.3}
$$

Next we evaluate $C(x)$ at control points x_m to get

$$
C(x_m) = \sum_{n=1}^{N} K_{mn} \, \ell_n \tag{2.3.4}
$$

with

$$
K_{mn} = \frac{1}{2\pi} \left[F(x_m - x_n^-) - F(x_m - x_n^+) \right] \tag{2.3.5}
$$

The control points and break points are chosen according to the cosine distribution

$$
x = -\cos\theta \tag{2.3.6}
$$

with equal spacing on θ. We have

$$
\begin{aligned}
\theta_n &= (n - 1/2)\pi / N, & \theta_n^{\pm} &= \theta_n \pm \pi / 2N \\
x_n &= -\cos\theta_n, & x_n^{\pm} &= -\cos(\theta_n \pm \pi / 2N)
\end{aligned}
\tag{2.3.7}
$$

The discrete kernels for the various problems of interest are summarized below:

Load equation (2.1.15)

$$\sum_{n=1}^{N} K_{mn}^{L}\,\ell_n = \alpha_m \qquad m = 1,\ldots,N$$

$$K_{mn}^{L} = \frac{1}{2\pi}\left[\ell n\left|\frac{x_m - x_n^-}{x_m - x_n^+}\right| + e^{\sigma(x_m - x_n^-)}K_0\left(\sigma\left|x_m - x_n^-\right|\right) - e^{\sigma\left(x_m - x_n^+\right)}K_0\left(\sigma\left|x_m - x_n^+\right|\right)\right]$$

$$c_L = \frac{\pi}{N}\sum_{n=1}^{N}\ell_n \sin\theta_n \tag{2.3.8}$$

High σ approximation (2.2.15)

$$\tilde{K}_{mn}^{L} = \frac{1}{2\pi}\left[\ell n\left|\frac{x_m - x_n^-}{x_m - x_n^+}\right| + \sqrt{\frac{\pi}{2\sigma}}\left(\frac{H\left(x_m - x_n^-\right)}{\sqrt{\left|x_m - x_n^-\right|}} - \frac{H\left(x_m - x_n^-\right)}{\sqrt{\left|x_m - x_n^-\right|}}\right)\right] \tag{2.3.9}$$

Universal load equation (2.1.39)

$$\sum_{n=1}^{N} K_{mn}^{D} F_n = 1 \tag{2.3.10}$$

$$K_{mn}^{D} = \frac{1}{2\pi}\left[K_0\left(\sigma\left|x_m - x_n^-\right|\right)\sinh\,\sigma\left(x_m - x_n^-\right) - K_0\left(\sigma\left|x_m - x_n^+\right|\right)\sinh\left(x_m - x_n^+\right)\right]$$

Also

$$\|F\| = \int_{-1}^{1} F(x)dx = \frac{\pi}{N}\sum_{n=1}^{N} F_n \sin\theta_n \tag{2.3.10}$$

so that

$$c_D = c_L^2 / \|F\|$$
$$\ell_n = c_L F_n / \|F\|$$
$$\alpha_n = \frac{c_L}{\|F\|} \sum_{n=1}^{N} K_{mn}^L F_n \tag{2.3.11}$$

where K_{mn}^L is given by (2.3.8).

High σ approximation (2.2.34)

$$\sum_{n=1}^{N} \tilde{K}_{mn}^D G_n = 1 \tag{2.3.12}$$

$$\tilde{K}_{mn}^D = \frac{1}{2\pi}\left[\frac{sgn(x_m - x_n^-)}{\sqrt{|x_m - x_n^-|}} - \frac{sgn(x_m - x_n^+)}{\sqrt{x_m - x_n^+}}\right]$$
$$\|G\| = \frac{\pi}{N}\sum_{n=1}^{N} G_n \sin\theta_n$$
$$c_D = \frac{1}{2}\sqrt{\frac{\pi}{2\sigma}}\, c_L^2 / \|G\|$$
$$\ell_n = c_L \cdot G_n / \|G\|$$
$$\alpha_n = \frac{c_L}{\|G\|} \cdot \sum_{n=1}^{N} \cdot K_{mn}^L \cdot G_n \tag{2.3.14}$$

with K_{mn}^L given by (2.3.9).

Section induced drag (2.1.31)

The inner kernel in (2.1.31) is precisely K_{mn}^D. Thus

$$c_D = \frac{\pi c_L^2}{N\|\ell\|^2} \sum_{m=1}^{N}\sum_{n=1}^{N} \ell_m \sin\theta_m K_{mn}^D \ell_n \tag{2.3.15}$$

$$\|\ell\| = \frac{\pi}{N}\sum_{n=1}^{N} \ell_n \sin\theta_n \tag{2.3.16}$$

High σ approximation (ℓ regular)

If the load is regular at the leading and trailing edges we can use the asymptotic approximation of K^D_{mn} in (2.3.14) to get,

$$c_D = \frac{\pi c_L^2}{2N\|\ell\|^2} \sum_{m=1}^{N} \sum_{n=1}^{N} \ell_m \sin\theta_m \tilde{K}^D_{mn} \ell_n \qquad (2.3.17)$$

with $\tilde{K}^D_{mn}$ given by (2.3.13).

All of the following numerical results were obtained with the above algorithm, except for the load and separation potential of the airfoil with flap. The modifications needed to handle the log singularity are discussed in Appendix A.

Constant Angle of Attack

The load distribution $\ell(x)$ and the induced drag angle $\alpha_d(x)$ are plotted in Figures 2-6a and b for σ = [.001, .1, 1.0, 10, 10000]. The load evolves from the low Reynolds number asymptotic form (see (2.2.5)) to the high Reynolds number form (see (2.2.19)) with the Kutta condition ($c_L = 2\pi\alpha$). The induced drag angle $\alpha_d(x)$ tends to a constant at low Reynolds number which indicates that the low Reynolds number section induced drag is locally proportional to the load. At high Reynolds number the induced drag angle becomes more and more concentrated near the leading edge. This reinforces our asymptotic result (see (2.2.48)) for the flat plate section drag, where we showed that the leading edge was the dominant viscous contribution. Also, see the summary results in Figure 2-9 below.

Parabolic camber

The load distribution and the induced drag angle for parabolic camber are plotted in Figures 2-7a and b. At low Reynolds number, the load tends to a nearly non-lifting form with fore and aft anti-symmetry, compared to the highly lifting angle of attack case. At high Reynolds number we again recover the elliptic load distribution that is obtained with inviscid theory and the Kutta condition. The induced drag angle is nearly linear over the section at low Reynolds number and virtually constant (nearly zero in Figure 2-7b) at high Reynolds number.

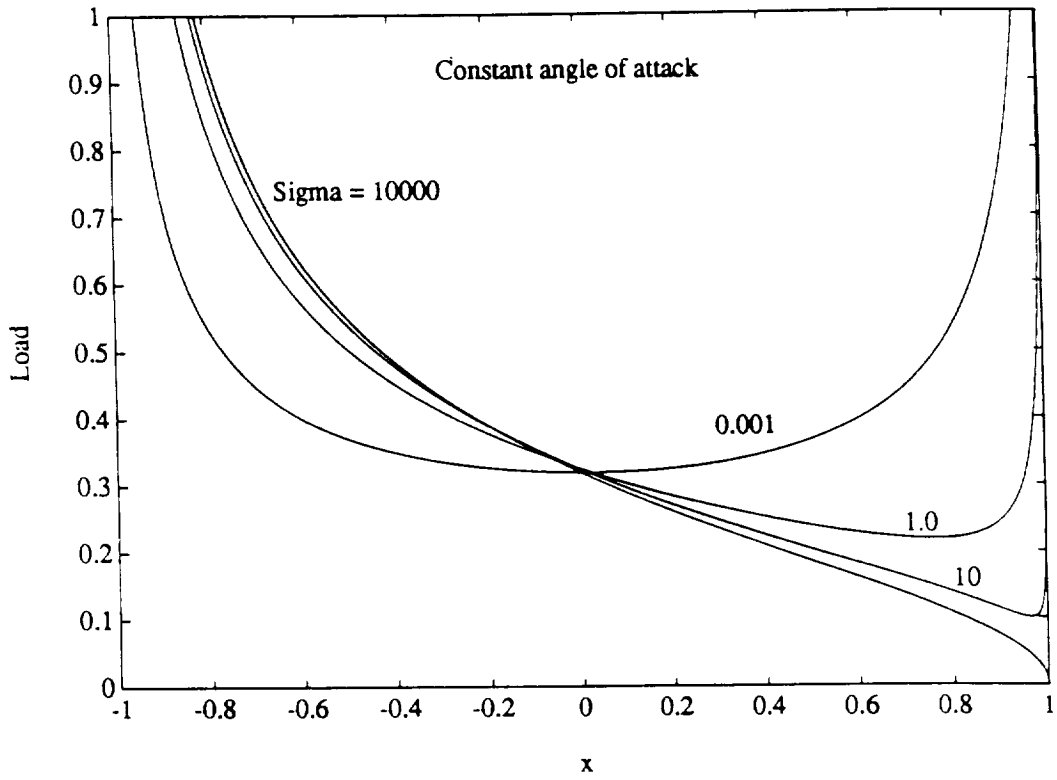

Figure 2-6a. Load distributions: Constant α; σ = [0.001 to 10000].

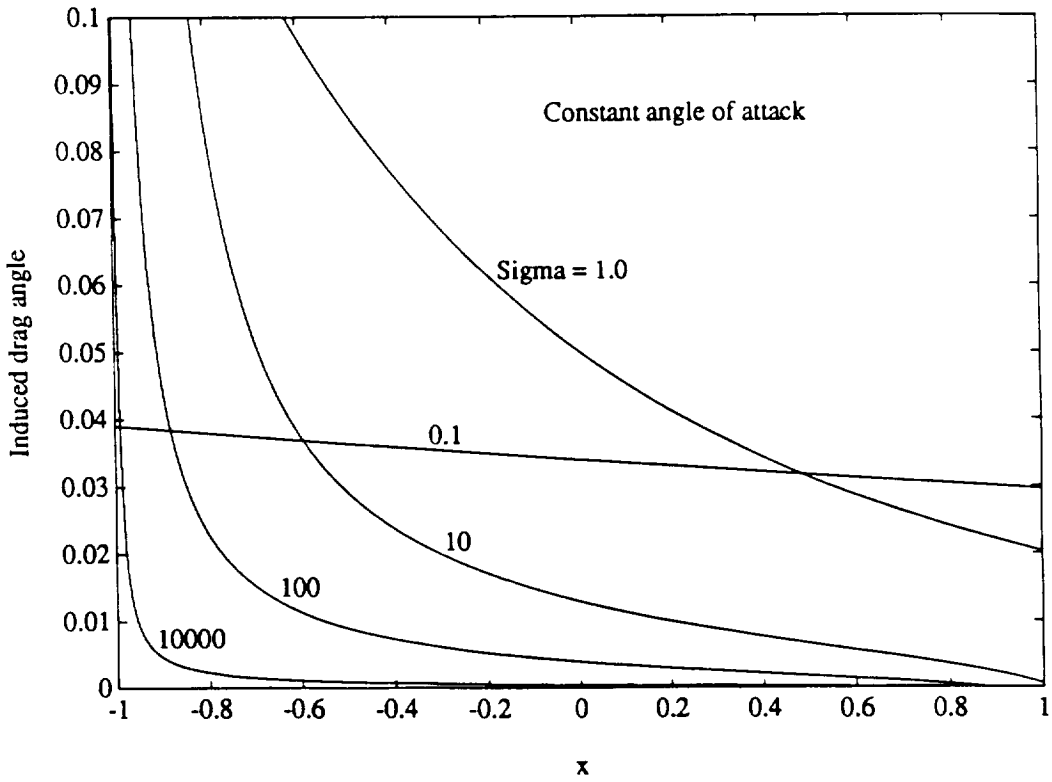

Figure 2-6b. Induced drag angle: Constant α; σ = [0.1 to 10000].

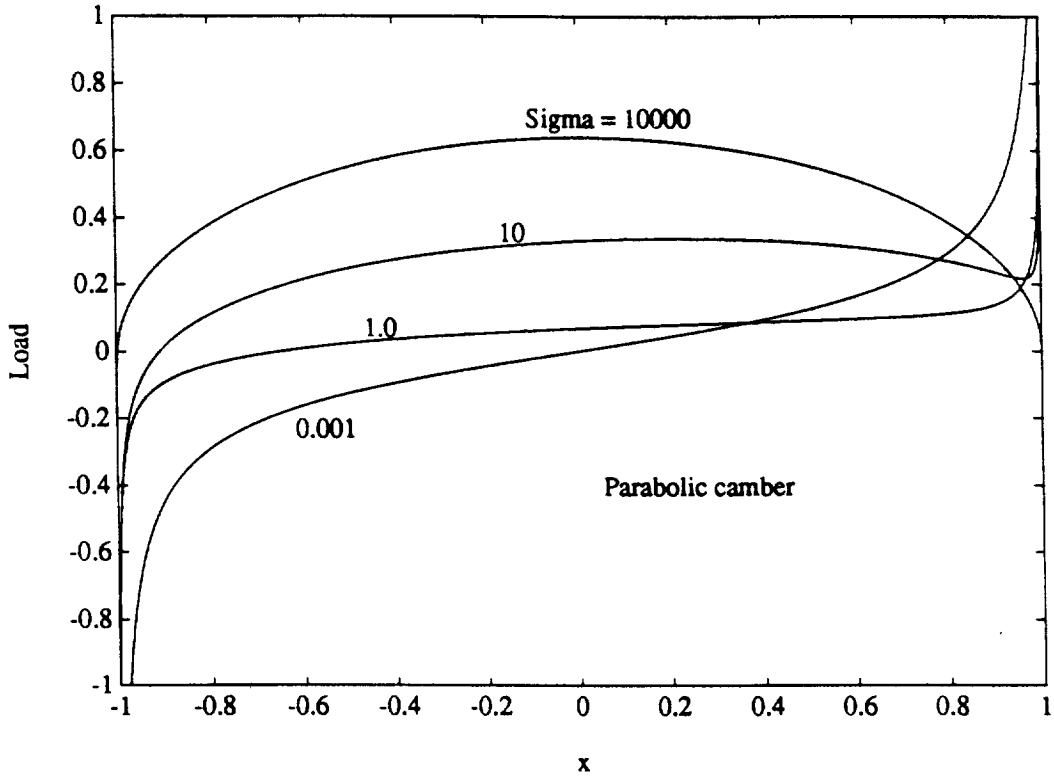

Figure 2-7a. Load distributions: Parabolic camber; σ = [0.001 to 10000].

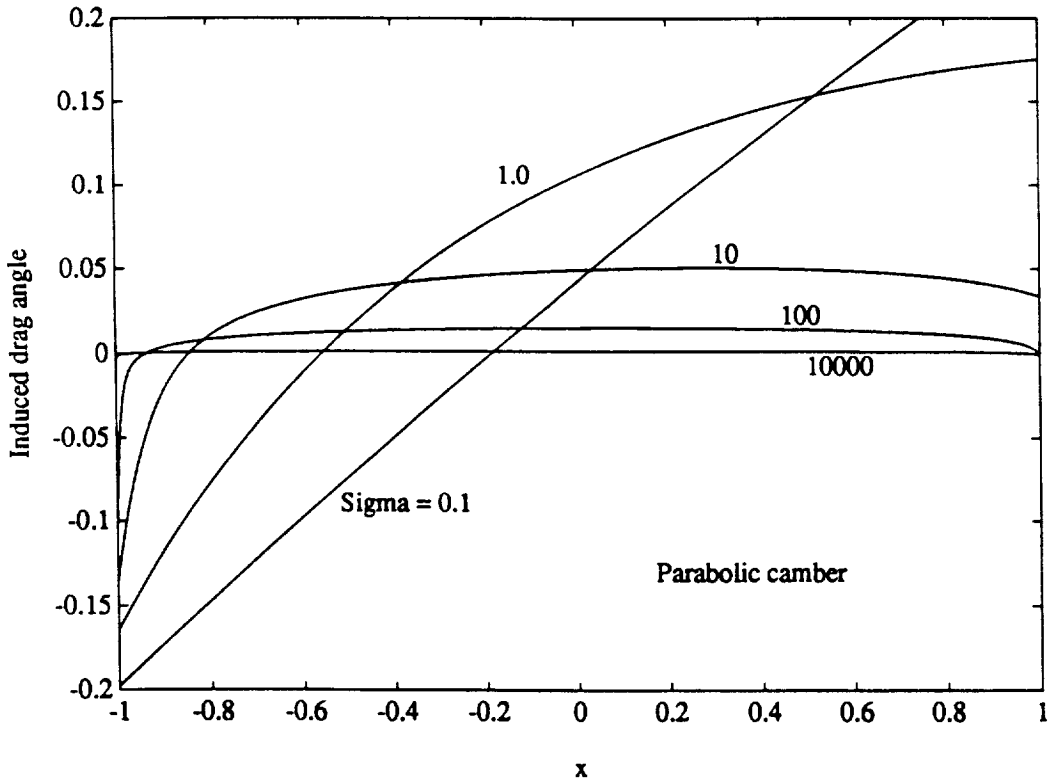

Figure 2-7b. Induced drag angle: Parabolic camber; σ = [0.1 to 10000].

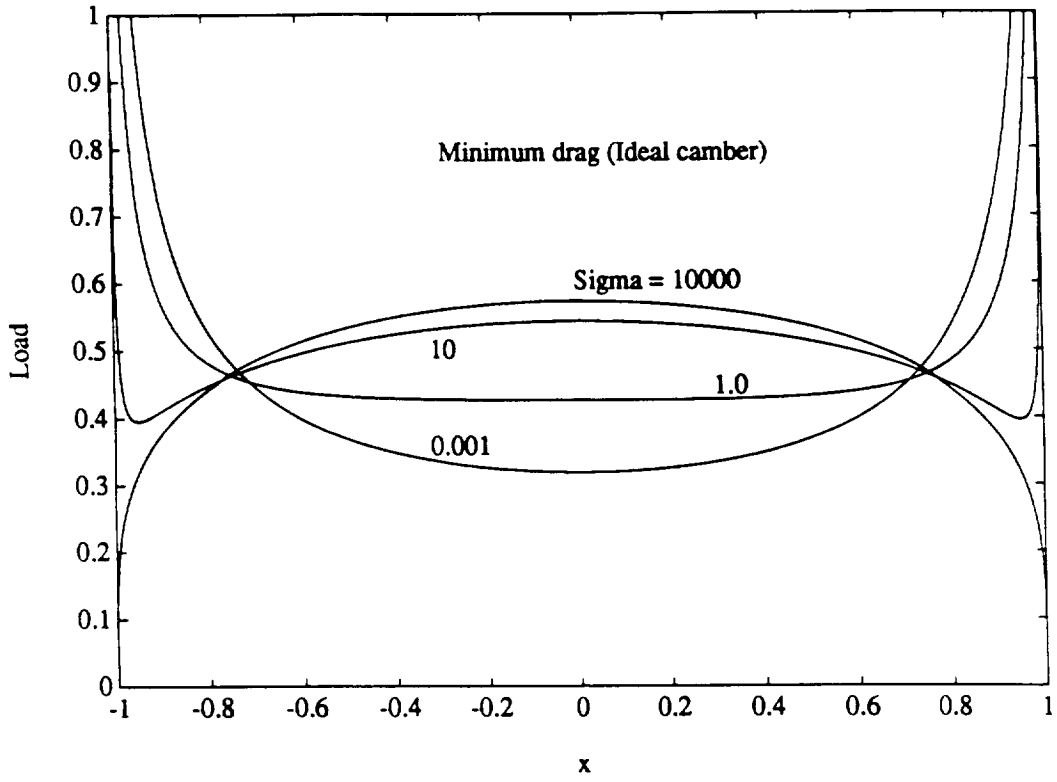

Figure 2-8a. Load distributions: Minimum drag; σ = [0.001 to 10000].

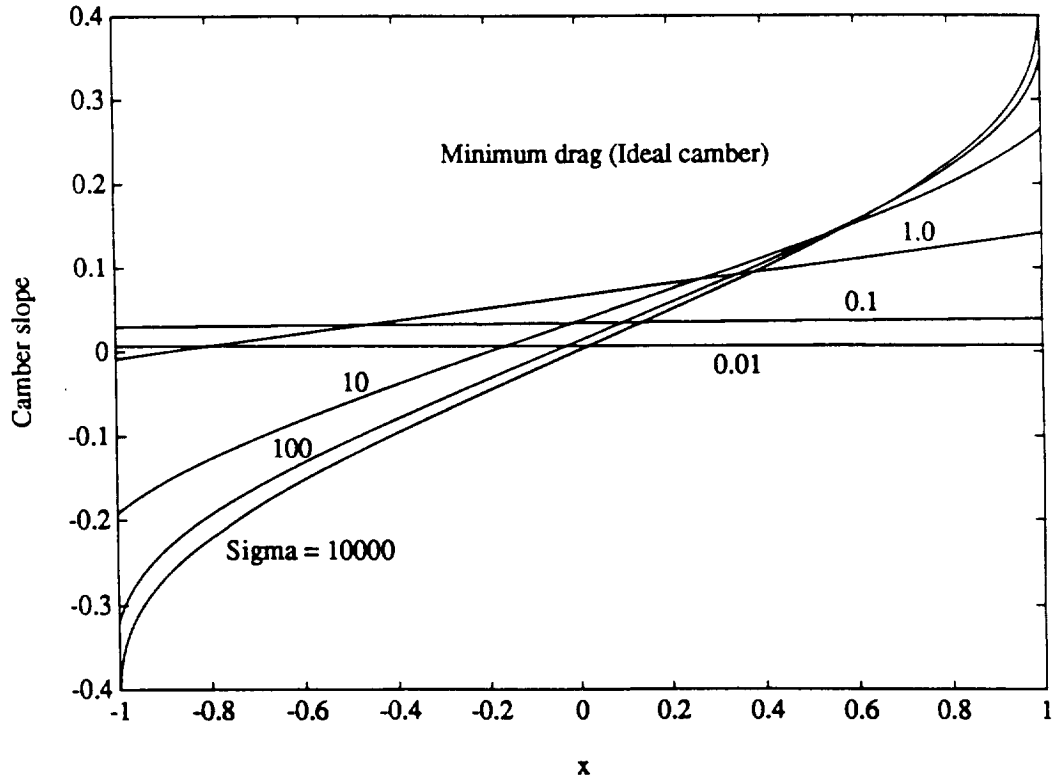

Figure 2-8b. Camber slope: Minimum drag; σ = [0.01 to 10000].

We will see below that the high Reynolds number results for parabolic camber are very close to those for the minimum drag solution.

Minimum drag solution

The load distribution and the local angle of attack or negative slope of the camber shape are plotted in Figures 2-8a and b. The section induced drag angle at minimum drag is a constant for any Reynolds number as we discussed in the derivation of these solutions. This important result is analogous to the 3-D minimum drag result wherein the downwash or induced angle of attack is constant across the span. The load distribution at minimum drag and $\sigma \to 0$ is identical to the solution for constant angle of attack. From Figure 2-8b we see that α = constant is the low Reynolds number camber shape in accordance with Batchelors theorem (see page 21). At high Reynolds number, the minimum drag solution tends to a more elliptic load distribution with a shape that has logarithmic cusps at the leading and trailing edge.

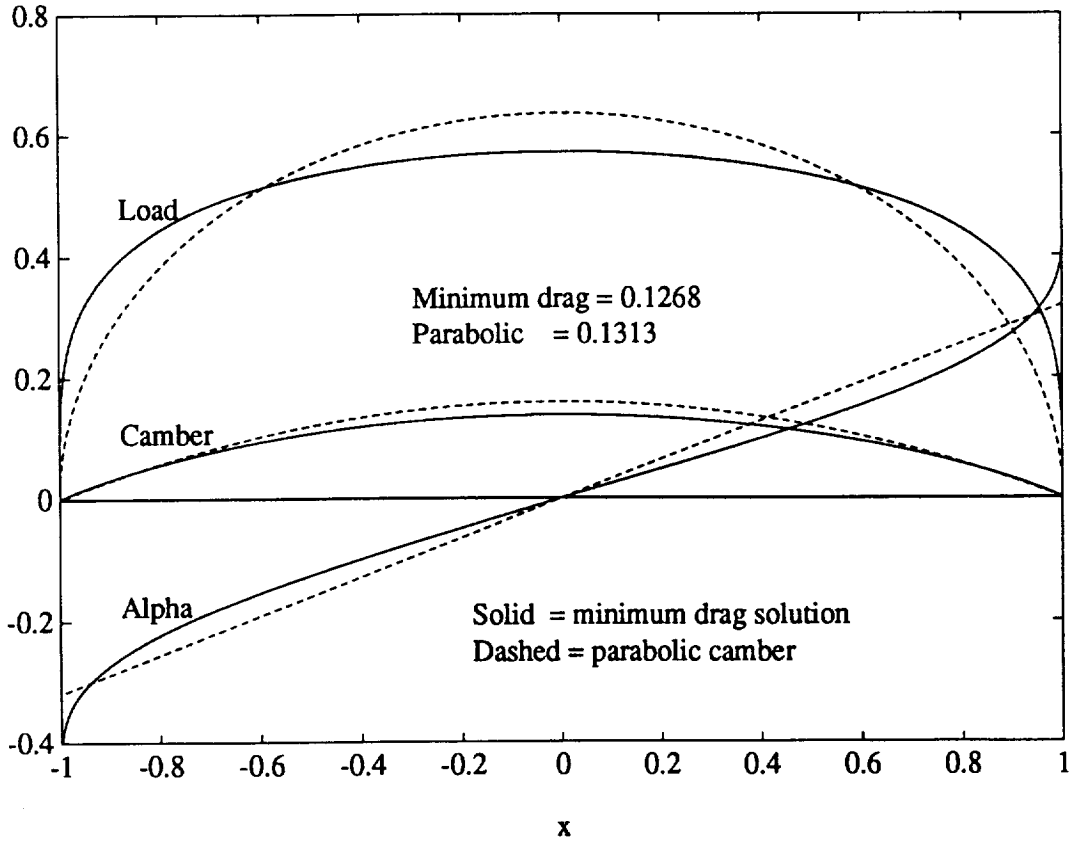

Figure 2-9. Comparison of minimum drag and parabolic camber loads and shape for very high Reynolds number σ.

We compare the minimum drag solution with the parabolic solution in Figure 2-9. These results were computed with the asymptotic formulation of the minimum drag problem (see (2.3.12) through (2.3.14)). The minimum drag shape has a steeper slope at the leading and trailing edges than the parabolic camber shape. The load distribution is also more concentrated at the edges. The limiting values of the section induced drag parameter $\sqrt{\sigma}\, c_D / c_L^2$ are 0.1268 and 0.1313 respectively for the minimum drag and parabolic camber configurations—about a 4 percent difference.

Lift and drag summary

We summarize the results for all three of the above configurations in Figures 2-10a and b over the Reynolds number range $\sigma = 10^{-3}$ to 10^4. Each configuration amplitude (alpha or the camber height) is set to yield a unit section lift coefficient for $\sigma \to \infty$. The constant alpha lift coefficient is singular for $\sigma \to 0$ in accordance with our asymptotic result (2.2.7). For parabolic camber it tends to a constant ($\cong$ 2.0). The ideal section lift is unity over the full range of Reynolds number. The section induced drag for constant alpha tends asymptotically to the ideal minimum drag for $\sigma \to 0$ and to the flat plate limiting value ($1/2\pi \cong 0.159$) for $\sigma \to \infty$. For parabolic camber the section induced drag becomes infinite at low Reynolds number and tends asymptotically to zero as $0.1313/\sqrt{\sigma}$ for high Reynolds number which is approximately 4 percent greater than the high Reynolds number minimum induced drag ($.1268/\sqrt{\sigma}$). A curious feature of the minimum drag curve is that the section induced drag, c_d / c_L^2 is a maximum for $\sigma = 1.0$.

2-D Separation potentials ($\sigma \to \infty$)

We conclude our presentation of 2-D numerical results with a comparison of the separation potentials for three camber configurations:

1. Angle of attack (9 degree)
2. Parabolic camber (8% chord)
3. Flap foil (20% chord at 16 degrees)

All configurations are for a section $c_L = 1.0$. The inviscid load distributions with Kutta condition are plotted in Figure 2-11 for convenient reference.

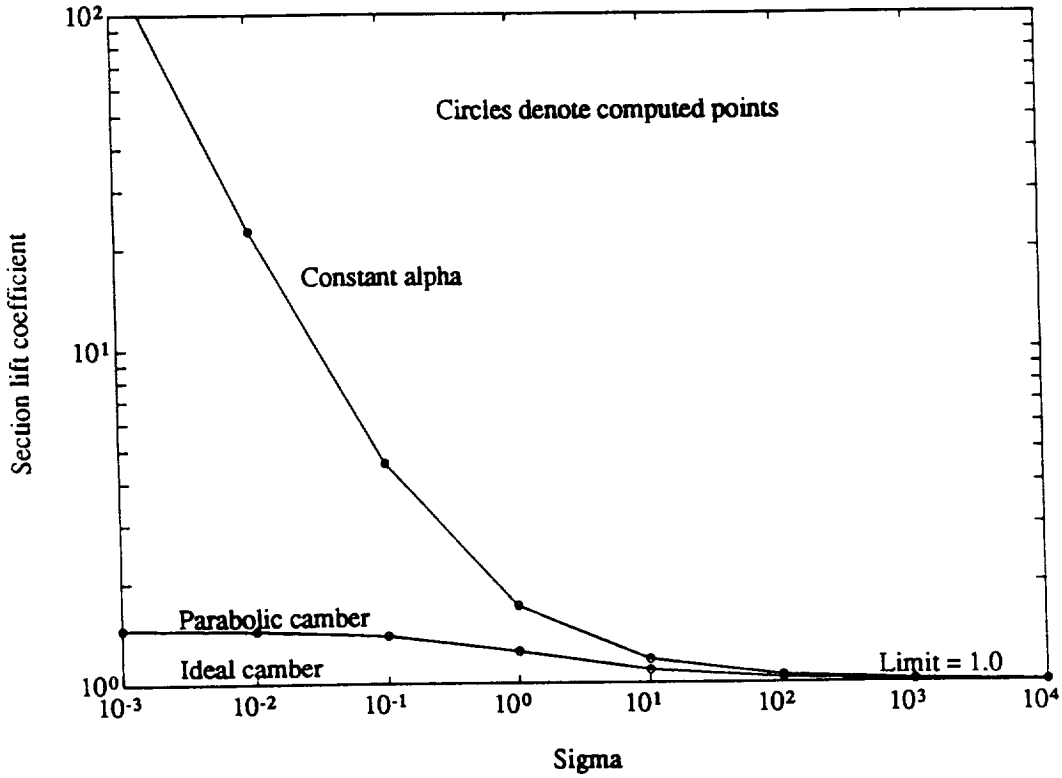

Figure 2-10a. Section lift coefficient versus Reynolds number σ for three geometries.

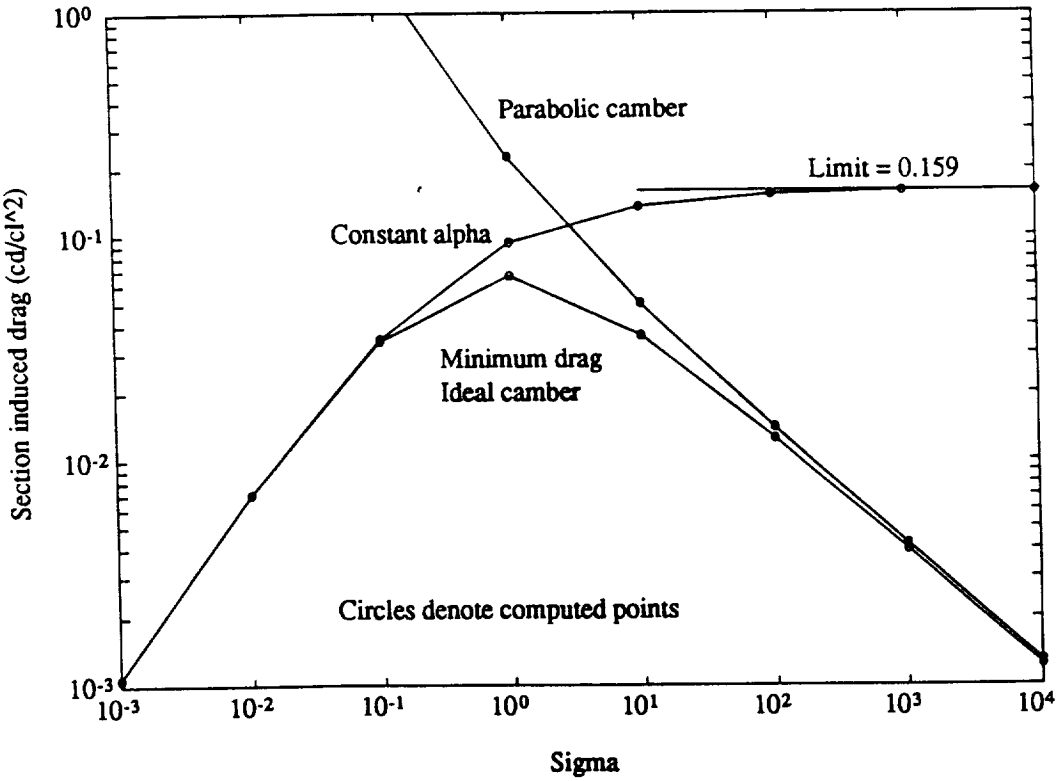

Figure 2-10b. Section induced drag versus Reynolds number σ for three geometries.

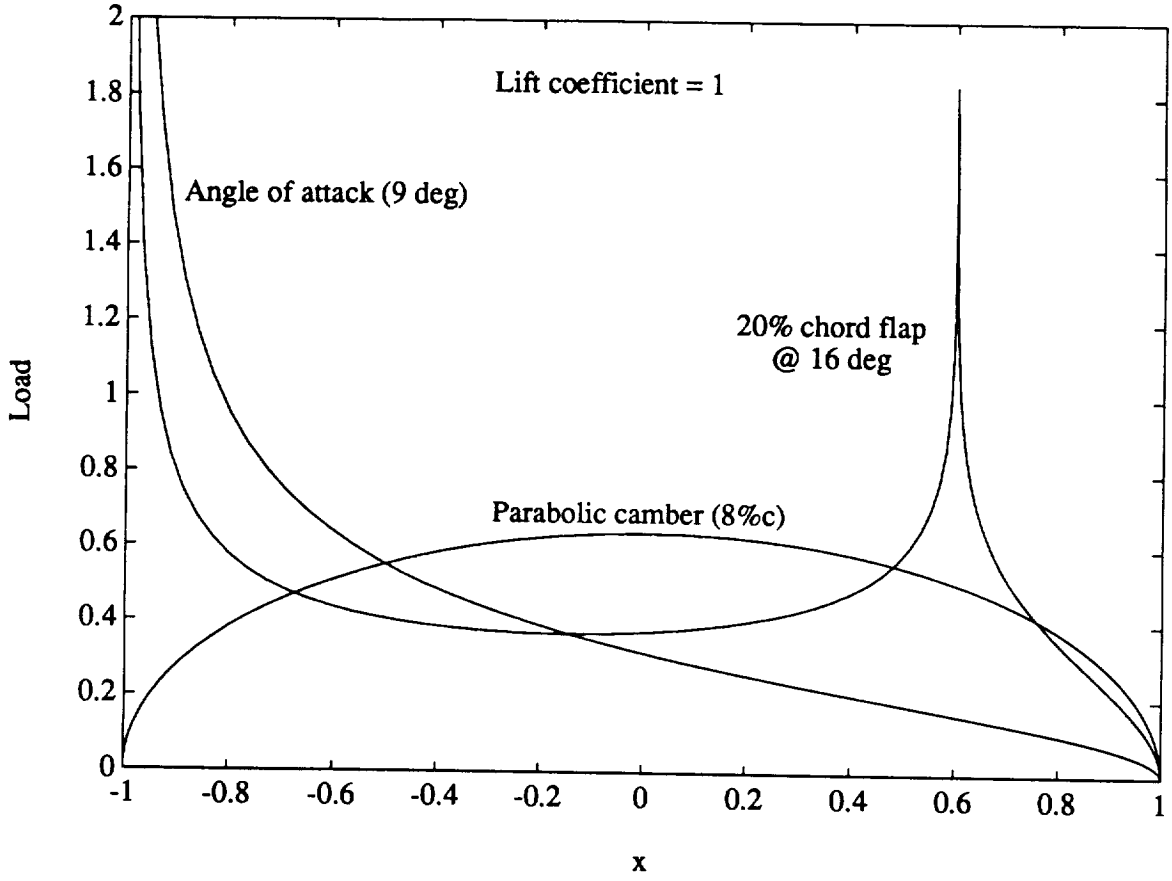

Figure 2-11. Inviscid (Kutta) load distributions for constant angle of attack, parabolic camber and 20% chord flap.

The normalized viscous induced camber, $\sqrt{\sigma}\, f_v$, and the normalized separation potential, $\sqrt{\sigma}\, \alpha_v$, in Figures 2-12a and b are calculated with the high Reynolds number numerical approach outlined in Appendix A. The results for angle of attack and parabolic camber are identical to results obtained with the analytic formulas (2.2.24) and (2.2.28). While the viscous induced camber shape indicates a separation problem at the flap hinge line the best overall indicator is the separation potential in Figure 2-12b. For case 1, constant angle of attack, the potential is positive over the entire chord with a logarithmically infinite value near the trailing edge. A very careful asymptotic analysis of the leading edge region for case 1 (not included herein) indicates an exponentially small region where $\sqrt{\sigma}\, \alpha_v$ is singular and positive. If we interpret a positive value as an indication of separation on the suction side and a negative value as an indication for separation on the compression side, case one is most susceptible to separation on the suction side near the trailing edge and near the leading edge.

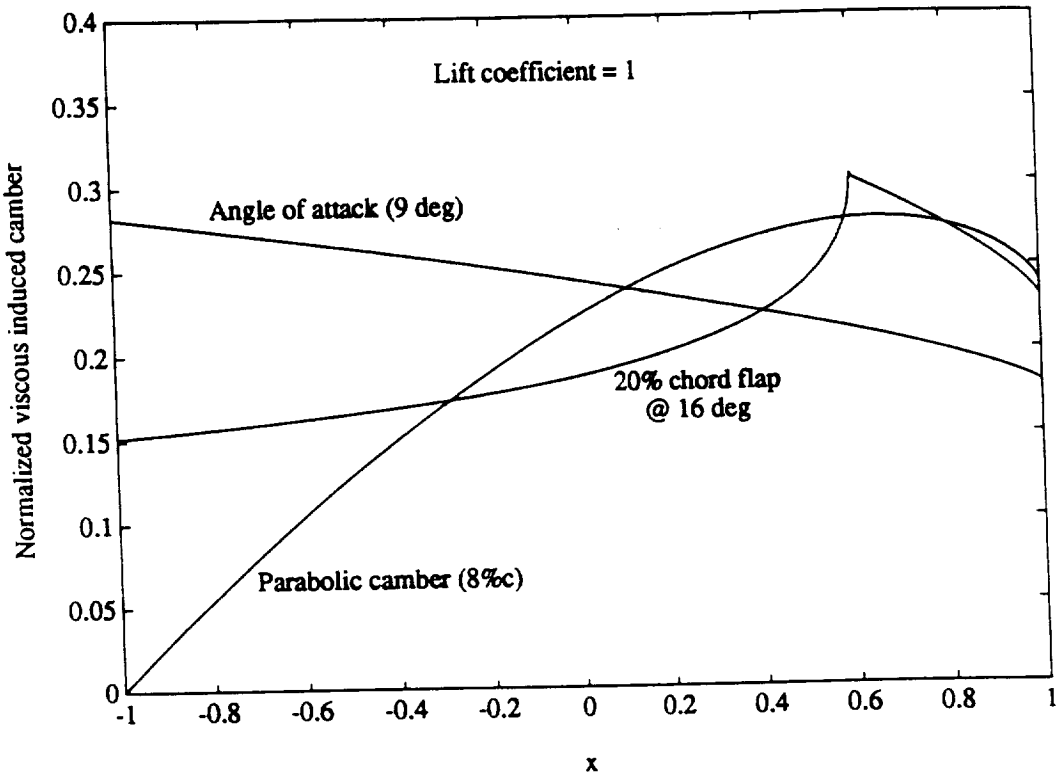

Figure 2-12a. Comparison of normalized viscous induced camber distributions.

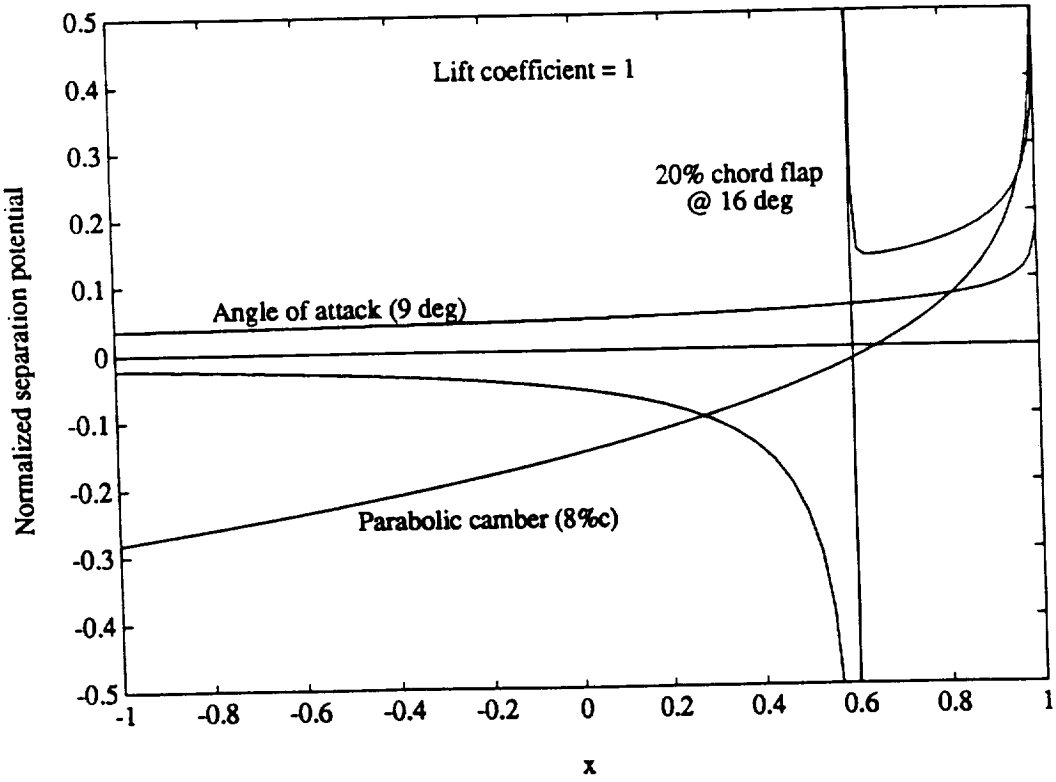

Figure 2-12b. Comparison of normalized separation potentials.

The relatively small value at $\sqrt{\sigma}\,\alpha_v$ over most of the section may indicate reattachment of the familiar leading edge separation bubble.

The parabolic camber shape is susceptible to separation on the compression side of the leading edge and on the suction side near the trailing edge. Also, the trailing edge has a logarithmically singular separation potential and is probably more susceptible than the leading edge. For the same lift coefficient, separation on the parabolic shape would occur before that on the constant alpha case.

The results for a foil section with flap are particularly interesting. The potential for separation near the leading edge is small but shifts to the compression side compared to the constant angle of attack case. Near the hinge line separation is indicated on the suction side downstream of the hinge line and on the compression side upstream of the hinge line. The trailing edge again exhibits the usual logarithmically singular potential for separation. We point out that these results are for a flap setting of 16 degrees which according to inviscid theory with Kutta would yield a unit lift coefficient. The strong indication and likely occurrence of separation near the hinge line is probably responsible for the reduced effectiveness of flaps. We suggest that the separation potential could perhaps be used as a theoretical tool for correlating experimental results on flap effectiveness with Reynolds number.

In conclusion we remark that no attempt was made to compute the section drag of the flap foil configuration herein. It is intuitively obvious however that large induced drag angles will result near the hinge line which together with the logarithmically singular load will result in a section drag penalty. These Reynolds dependent effects can be computed with the present theory.

III. Complete Viscous Theory of the 3-D Thin Wing

3.1 Basic Analysis

The remarkable feature of the present theory is that the entire program can be carried out for a 3-D thin wing configuration. Most of the arguments follow from the 2-D case and will not be repeated in detail. Some features are quite different and will be noted. Some of the results derived herein may also be found in the AIAA lecture notes (Yates 1990).

The "*belt sander*" concept is again used to remove the primary boundary layer. Using vector notation, the perturbation viscous problem and boundary conditions are (see (2.1.2)):

$$\begin{aligned} &\operatorname{div}\vec{\mathrm{v}} = 0 \\ &\frac{\partial \vec{\mathrm{v}}}{\partial x} + \operatorname{grad} p = -\frac{1}{2\sigma}\operatorname{curl}\vec{\omega} \\ &\vec{\omega} = \operatorname{curl}\vec{\mathrm{v}} \qquad \operatorname{div}\vec{\omega} = 0 \\ \text{On}\quad S: &\; u = \mathrm{v} = 0, \qquad w = \frac{\partial f}{\partial x} = -\alpha(x,y) \end{aligned} \tag{3.1.1}$$

where all dimensionless quantities are defined as in Section 2. The length c is the mean aerodynamic chord

$$c = \frac{S}{b} = \frac{b}{A} \tag{3.1.2}$$

where b is the span, S is the planform area and A is the aspect ratio. Alternatively, we can write the problem in terms of pressure and vorticity:

$$\begin{aligned} &\nabla^2 p = 0 \\ &\frac{\partial \vec{\omega}}{\partial x} = \frac{1}{2\sigma}\nabla^2\vec{\omega} \qquad \operatorname{div}\vec{\omega} = 0 \\ \text{On}\quad S: &\qquad \omega_z = \frac{\partial \mathrm{v}}{\partial x} - \frac{\partial u}{\partial y} = 0 \end{aligned} \tag{3.1.3}$$

which implies that $\omega_z = 0$ everywhere and we have,

$$\frac{\partial p}{\partial x} = \frac{1}{2\sigma}\frac{\partial \omega_y}{\partial z}$$

$$\frac{\partial p}{\partial y} = -\frac{1}{2\sigma}\frac{\partial \omega_x}{\partial z}$$

$$\frac{\partial^2 f}{\partial x^2} + \frac{\partial p}{\partial z} = \frac{1}{2\sigma}\left(\frac{\partial \omega_x}{\partial y} - \frac{\partial \omega_y}{\partial z}\right) \tag{3.1.4}$$

These boundary conditions are fundamental as we have discussed before (Yates 1990). The first two equations show how a pressure gradient along the surface produces vorticity transverse to the gradient—a viscous micro version of Prandtl's wing theory. The last equation shows how viscosity modifies the balance of the normal pressure gradient at the surface. This boundary condition is responsible for the viscous correction to the usual inviscid load-downwash kernel as we will see below.

With the integral momentum and energy balance discussed by Yates 1990, we obtain two remarkable equations for the resultant lift and drag-due-to-lift:

$$C_L = \frac{L}{\frac{1}{2}\rho U_\infty^2 S} = \frac{1}{2A}\int_T dydz\ \omega_x \cdot y \tag{3.1.5}$$

$$C_D = \frac{D}{\frac{1}{2}\rho U_\infty^2 S} = \frac{1}{4A\sigma}\int_V dV\left(\omega_x^2 + \omega_y^2\right) \tag{3.1.6}$$

where T is the Trefftz plane and V is the entire volume of fluid. The drag formula is quadratic in the two nonzero components of the interactive vorticity while the lift is linear in ω_x. This will lead directly to the well-known quadratic relation between lift and drag.

An important difference between the 2-D and 3-D problems is that the latter has two components of vorticity. Fortunately, we can represent ω_x and ω_y in terms of a single function. Since

$$\frac{\partial \omega_x}{\partial x} + \frac{\partial \omega_y}{\partial y} = 0 \tag{3.1.7}$$

we let

$$\omega_x = \frac{\partial B}{\partial y} \qquad \omega_y = -\frac{\partial B}{\partial x} \tag{3.1.8}$$

where B is like a vorticity stream function. With (3.1.3) we note that B must satisfy the diffusion equation

$$\frac{\partial B}{\partial x} = \frac{1}{2\sigma}\nabla^2 B \tag{3.1.9}$$

The fundamental solutions for p and B can be used to represent the general solution in terms of unknown source strengths q_0 and q_1:

$$\begin{aligned} p &= \frac{\partial}{\partial y}\iint_S d\xi d\eta \, \frac{q_0(\xi,\eta)}{R} \\ B &= \iint_S d\xi d\eta \, q_1(\xi,\eta)\cdot\frac{e^{\sigma(x-\xi-R)}}{R} \end{aligned} \tag{3.1.10}$$

with

$$R = \left[(x-\xi)^2 + (y-\eta)^2 + z^2\right]^{1/2} \tag{3.1.11}$$

Compute the limit of p and $\frac{\partial B}{\partial z}$ as $z \to 0\pm$ on S to obtain

$$\begin{aligned} p(x,y,0\pm) &= \mp 2\pi q_0(x,y) \\ \left.\frac{\partial B}{\partial z}\right|_{z=0\pm} &= \mp 2\pi q_1(x,y) \end{aligned} \tag{3.1.12}$$

Introduce the load function

$$\ell(x,y) = p(0^-) - p(0^+) = 4\pi q_0 \tag{3.1.13}$$

Next we use the x momentum equation

$$\frac{\partial u}{\partial x} + \frac{\partial p}{\partial x} = \frac{1}{2\sigma}\frac{\partial \omega_y}{\partial z} = -\frac{1}{2\sigma}\frac{\partial}{\partial x}\frac{\partial B}{\partial z}$$

to get

$$u = -\left(p + \frac{1}{2\sigma}\frac{\partial B}{\partial z}\right) \tag{3.1.14}$$

Since u must be zero on S we obtain

$$p(x,y,0\pm) = -\frac{1}{2\sigma}\frac{\partial B}{\partial z}\bigg|_{z=0\pm} \tag{3.1.15}$$

which with (3.1.12) and (3.1.13) yields the source strengths q_0 and q_1 in terms of ℓ

$$q_0 = \frac{\ell(x,y)}{4\pi} \qquad q_1 = -\frac{\sigma\ell(x,y)}{2\pi} \tag{3.1.16}$$

The y momentum equation

$$\frac{\partial v}{\partial x} = -\frac{\partial}{\partial y}\left(p + \frac{1}{2\sigma}\frac{\partial B}{\partial z}\right) \tag{3.1.17}$$

with (3.1.14) shows that $v = 0$ on S. The representations for p and B are

$$p = \frac{1}{4\pi}\iint_S d\xi d\eta \frac{\ell}{R}$$

$$B = -\frac{\sigma}{2\pi}\iint_S d\xi d\eta \cdot \ell \frac{e^{\sigma(x-\xi-R)}}{R}$$

$$\omega_x = \frac{\partial B}{\partial y} \qquad \omega_y = -\frac{\partial B}{\partial x} \tag{3.1.18}$$

Finally, we combine these representations in the vertical momentum equation, integrate from $-\infty$ to x and use the boundary condition on w to get the 3-D wing load equation,

$$\frac{1}{4\pi}\iint_S d\xi d\eta \, \ell \, K_L(x-\xi, y-\eta) = -\alpha \tag{3.1.19}$$

with

$$K_L = \frac{\partial}{\partial x}\left(\frac{1-e^{\sigma(x-R)}}{R}\right) - \frac{\partial}{\partial y}\left[\frac{1}{y}\left(1+\frac{x}{R}\right)(1-e^{\sigma(x-R)})\right] \tag{3.1.20}$$

The inviscid and viscous load kernels $K_L(x,y)$ are plotted in Figure 3-1a and b respectively on Reynolds scaled coordinates $X = \sigma x$, $Y = \sigma y$. Each kernel is the upwash

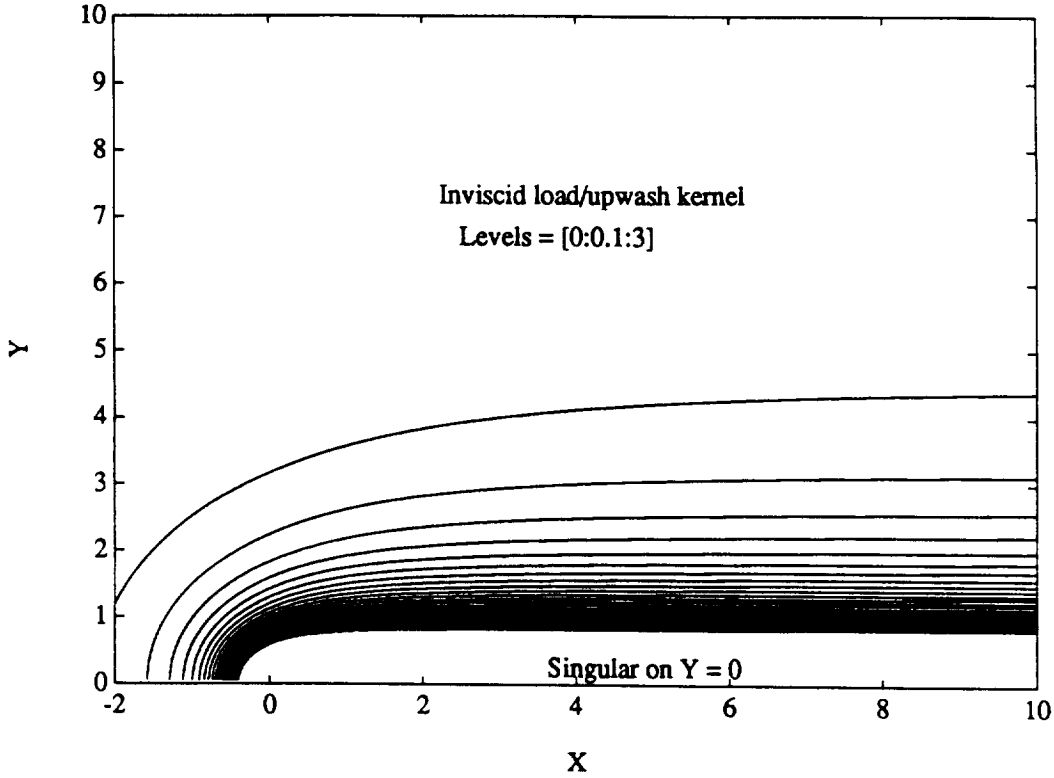

Figure 3-1a. Contour plot of the inviscid load/upwash kernel function.

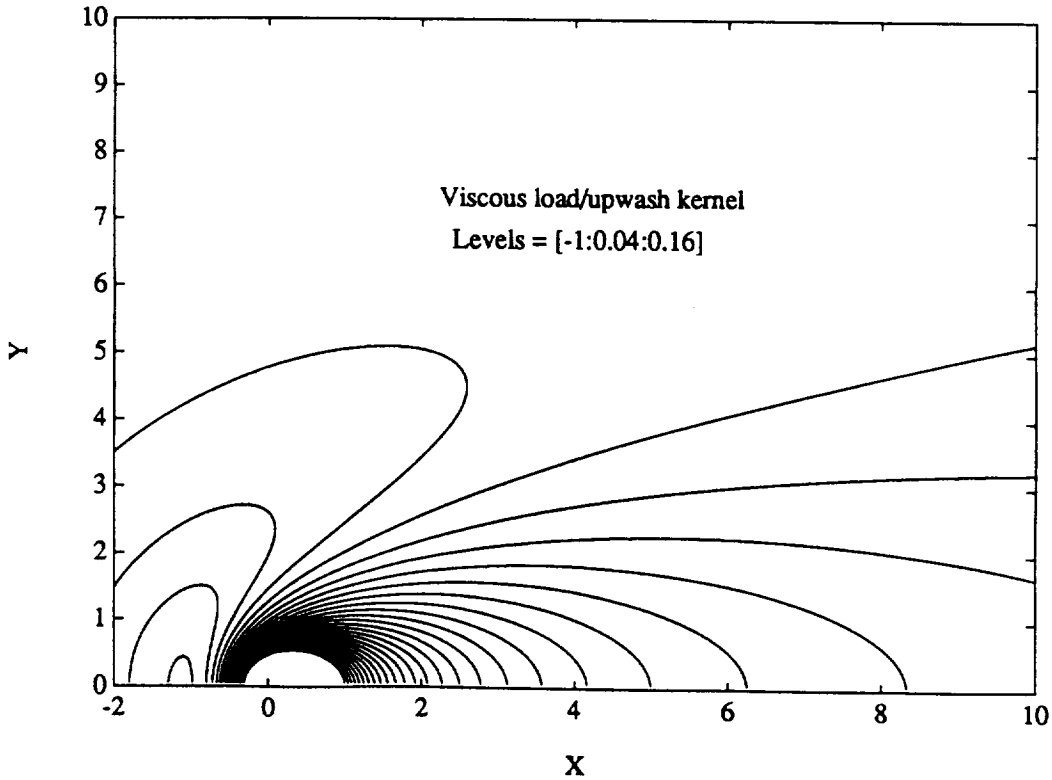

Figure 3-1b. Contour plot of the viscous load/upwash kernel function.

induced by a point load at the origin. Note that the inviscid kernel is much more singular than the viscous kernel. Also, we point out that the complete structure of the viscous kernel is buried on the scale of $1/\sigma$ inside the singular region of the inviscid kernel.

Resultant lift

It is instructive to derive an expression for the resultant lift in terms of ℓ using the vorticity relation (3.1.5) and the integral representation of ω_x. We get

$$C_L = -\frac{1}{2A}\cdot\frac{\sigma}{2\pi}\iint_S d\xi d\eta\cdot\ell\cdot e^{\sigma(x-\xi)}\iint_{T(x)} dydz\, y\frac{\partial}{\partial y}\frac{e^{-\sigma R}}{R} \tag{3.1.21}$$

But

$$\int_T dydz\,\frac{e^{-\sigma R}}{R} = \int_0^{2\pi} d\theta\int_0^{\infty} rdr\,\frac{e^{-\sigma\left(x^2+r^2\right)^{1/2}}}{\left(x^2+r^2\right)^{1/2}} = \frac{2\pi}{\sigma}e^{-\sigma|x|} \tag{3.1.22}$$

so that for x downstream of any point on S we obtain

$$C_L = \frac{1}{2A}\iint_S \ell\, dxdy \tag{3.1.23}$$

which is the correct dimensionless representation of the lift coefficient in terms of the pressure jump or load ℓ.

Drag-due-to-lift

One of the most remarkable features of the 3-D viscous wing theory is that the drag coefficient (3.1.6) can be evaluated explicitly in terms of the load function just as it was in the 2-D problem. The derivation is given in detail in Appendix B. Here we record the final result

$$\begin{aligned} C_D = &-\frac{1}{8\pi A}\iint_S dxdy\frac{\partial\ell}{\partial y}\cdot\iint_S d\xi d\eta\frac{\partial\ell}{\partial\eta}K_D(x-\xi,y-\eta) \\ &-\frac{1}{8\pi A}\iint_S dxdy\frac{\partial\ell}{\partial x}\cdot\iint_S d\xi d\eta\frac{\partial\ell}{\partial\xi}\cdot K_D(x-\xi,y-\eta) \end{aligned} \tag{3.1.24}$$

with

$$K_D(x,y) = \ell n|y-\eta| + K_E(x,y)$$

$$K_E(x,y) = \frac{1}{2}[E(\sigma(R-|x|)) + E_1(\sigma(R+|x|))] \qquad (3.1.25)$$

$$E_1(z) = \int_z^\infty dt \frac{e^{-t}}{t} \qquad (3.1.26)$$

the standard exponential integral. This is perhaps the single most important result presented in this report. The drag-due-to-lift is a correlation of the spanwise and chordwise gradients of the load in the viscous induced drag kernel K_D—not too surprising since the load gradients are the source of all vorticity which contribute to the drag. This important induced drag kernel is plotted in Figure 3-2 with respect to Reynolds scaled coordinates $X = \sigma x$, $Y = \sigma y$ to reveal the viscous structure.

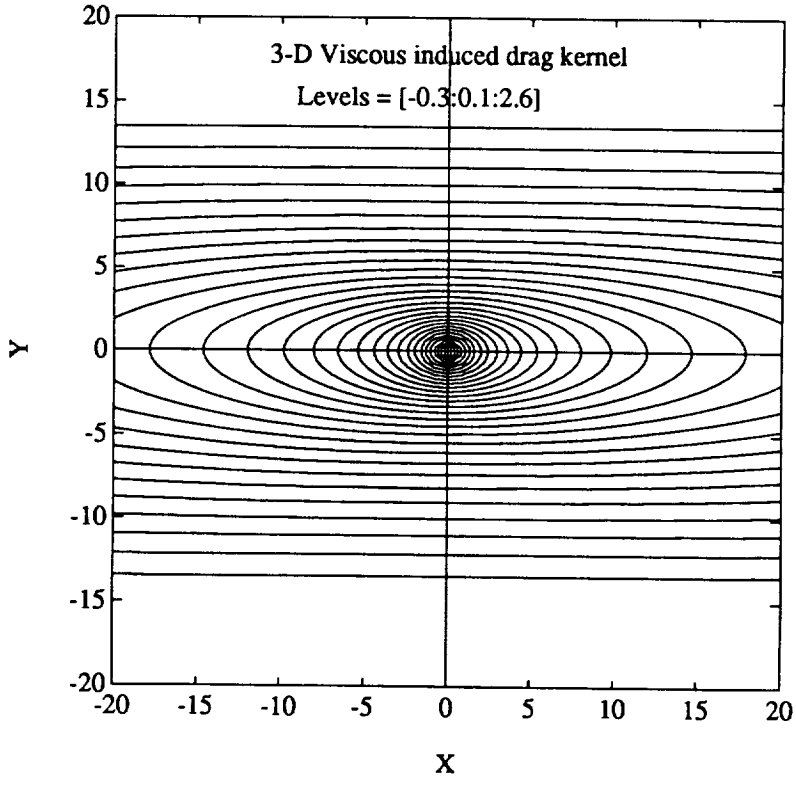

Figure 3-2. Contour plot of the viscous induced drag kernel function.

If we drop all terms that depend on the Reynolds number σ we obtain one representation of the classical induced drag that depends only on the spanwise load gradients; i.e.,

$$C_{D_{\text{classical}}} = -\frac{1}{8\pi A}\iint_S dxdy\frac{\partial \ell}{\partial y}\iint_S d\xi d\eta \frac{\partial \ell}{\partial \eta}\ell n|y-\eta|$$

$$= -\frac{1}{8\pi A}\int_b dy\,\frac{\partial L}{\partial y}\int_b d\eta \frac{\partial L}{\partial \eta}\ell n|y-\eta| \qquad (3.1.27)$$

with the span loading

$$L = \int_{c(y)} \ell(x,y)dx \qquad (3.1.28)$$

The "inviscid" logarithmic kernel in (3.1.27) cooresponds to the horizontal lines in the plot of Figure 3-2. For the elliptic span load distribution it is easily verified that (3.1.27) yields the well-known minimum drag result

$$C_{D_{\substack{\text{classical}\\ \text{minimum}}}} = \frac{C_L^2}{\pi A} \qquad (3.1.29)$$

independent of the details of the chordwise load distribution and the Reynolds number. We re-emphasize the point that we have derived this well-known result via the formula (3.1.6) that is unquestionably of viscous origin! All drag by whatever name we may give it is of viscous origin.

Another immediate result can be obtained with (3.1.24) if we assume that the span becomes infinite and $\frac{\partial \ell}{\partial y} = 0$. Then the first integral is zero and the y integral of K_E can be evaluated to obtain our previous result (2.1.31) for the section drag due to lift. We have already demonstrated the power of the 2-D theory in establishing the optimal chordwise load distribution to minimize section drag. Also we derived a Reynolds independent drag component for the flat plate at angle of attack—the leading edge suction. The formula

(3.1.24) combines all of these features in a single expression for the drag-due-to-lift that is Reynolds number dependent.

Comment on Greene's "viscous induced drag"

G.C. Greene (1988) proposed a modification of the traditional approach to the minimum induced drag problem that in principle uses the fundamental formula for drag in terms of enstrophy and the vorticity production formulas in terms of pressure gradients. Instead of minimizing the drag, however, he minimized the streamwise vorticity production by minimizing the square of the span load gradient which he incorrectly claims is the drag. The resultant span load is certainly not elliptic but the drag is also not a minimum. Furthermore, Greene's formulation does not reveal any of the coupled spanwise/chordwise structure of the viscous induced drag kernel in Figure 3-2.

Minimum drag-due-to-lift

The analysis of minimum drag and optimal wing loading is straightforward with the above formula for C_D. We construct the functional on ℓ,

$$J[\ell] = C_D[\ell] - \lambda\left(\frac{1}{2A}\iint_S dxdy\,\ell - C_L\right) \tag{3.1.30}$$

where λ is a Lagrange multiplier for the constraint on C_L. The variation of (3.1.30) yields the Euler equation for optimal wing loading. Eliminating the Lagrange multiplier we obtain the following results that may be compared with those in Section 2.1:

$$\frac{1}{4\pi}\nabla^2\iint_S d\xi d\eta \cdot F \cdot K_D(x-\xi, y-\eta) = 1 \tag{3.1.31}$$

with

$$\nabla^2 = \frac{\partial^2}{\partial x^2} + \frac{\partial^2}{\partial y^2}$$

$$C_D = \frac{2A}{\|F\|} C_L^2$$

$$\ell(x,y) = 2AC_L \, F(x,y) / \|F\|$$

$$\|F\| = \iint_S F \, dxdy \tag{3.1.33}$$

The optimal local angle of attack or camber slope distribution is given by

$$\alpha(x,y) = -\frac{1}{4\pi} \iint_S d\xi d\eta \cdot \ell \cdot K_L \tag{3.1.34}$$

where K_L is given by (3.1.20). For a given planform the above theory will yield the optimal load distribution and camber shape both spanwise and chordwise. Classical minimum drag theory or Greene's modification can only yield information about the span load distribution.

Separation potential

By inspection of the load-downwash relation (3.1.19), we observe that the inviscid and viscous parts of the kernel function K_L are separable if we introduce some device for omitting the neighborhood of the stronger singularity of the two individual parts (e.g., Hadamard finite part). Thus, we can define a 3-D viscous induced angle or separation potential α_v. We write

$$\frac{1}{4\pi} \iint_S d\xi d\eta \cdot \ell \cdot K_{\text{inv}} = -(\alpha + \alpha_v) \tag{3.1.35}$$

with

$$\alpha_v = \frac{1}{4\pi} \iint_S d\xi d\eta \cdot \ell \cdot K_v \tag{3.1.36}$$

and

$$K_v = -\frac{\partial}{\partial x} \frac{e^{\sigma(x-R)}}{R} + \frac{\partial}{\partial y} \left[\frac{1}{y} \left(1 + \frac{x}{R} \right) e^{\sigma(x-R)} \right] \tag{3.1.37}$$

The usual inviscid kernel is,

$$K_{\text{inv}} = \frac{\partial}{\partial x}\frac{1}{R} - \frac{\partial}{\partial y}\left[\frac{1}{y}\left(1+\frac{x}{R}\right)\right] \tag{3.1.38}$$

Our main interest here is in the separation potential α_v. We introduce a doublet strength $\Delta\varphi$ such that

$$\ell = -\frac{\partial \Delta\varphi}{\partial x} \tag{3.1.39}$$

where $\Delta\varphi$ is zero on the leading edge of S and takes on the value $\Delta\varphi_e$ at the trailing edge where

$$\Delta\varphi_e = -\int_{c(y)} \ell(x,y)dx = -L(y) \tag{3.1.40}$$

Integrate by parts in (3.1.36) and use the above results to get

$$\alpha_v(x,y) = \frac{1}{4\pi}\int_b d\eta\, L(\eta)K_v^e + \frac{1}{4\pi}\nabla^2 \iint_S d\xi d\eta\, \Delta\varphi \frac{e^{\sigma(x-\xi-R)}}{R} \tag{3.1.41}$$

where K_v^e is the viscous kernel (3.1.37) for source points on the trailing edge ($\xi = x_e(\eta)$). Explicit examples of the separation potential are given in Section 3. For high Reynolds number, it provides a powerful new tool for assessing the practicality of planform geometries and selected camber distributions.

3.2 High Reynolds number results

At present the status of the 3-D theory is incomplete. Many examples remain to be calculated and derived asymptotically to complete the program. Nevertheless, we present some key results at high Reynolds number that illustrate the utility of the viscous analysis.

When $\sigma >> 1$, the various viscous kernels in Section 3.1 become highly banded in the spanwise direction. For example, consider the viscous kernel (3.1.37) or the integrand in (3.1.41). The object

$$\frac{e^{\sigma(x-\xi-R)}}{R}$$

decays exponentially for $\sigma|y-\eta| >> 1$. In fact the relation $\sigma(x-\xi-R) = C$ defines a viscous parabolic zone of influence that opens downstream of the source point (ξ,η). Thus the object has the behavior of a delta function and we write

$$\frac{e^{-\sigma R}}{R} = C\delta(y) \tag{3.2.1}$$

with

$$C = \int_{-\infty}^{\infty} dy \frac{e^{-\sigma R}}{R} = 2K_0(\sigma|x|) \tag{3.2.2}$$

which reminds us of our previous 2-D results. With the above we can write

$$\begin{aligned} K_v \equiv & -2\delta(y)\frac{\partial}{\partial x} e^{\sigma x} K_0(\sigma|x|) \\ & -2\delta''(y)\int_{-\infty}^{x} d\xi e^{\sigma\xi} K_0(\sigma|\xi|) \end{aligned} \tag{3.2.3}$$

We further note that for $x < 0$, K_v becomes exponentially small on the scale of $1/\sigma$. Thus we can neglect the first term in the separation potential (3.1.41) and write

$$\alpha_v(x,y) \equiv \frac{1}{2\pi}\nabla^2 \iint_S d\xi d\eta \Delta\varphi e^{\sigma(x-\xi)} K_0(\sigma|x-\xi|)\delta(y-\eta) \tag{3.2.4}$$

Finally, we replace the Bessel function by its asymptotic approximation to get

$$\alpha_v(x,y) = \frac{1}{2\sqrt{2\pi\sigma}}\nabla^2 \cdot \int_{x_o(y)}^{x} d\xi \cdot \frac{\Delta\varphi(\xi,y)}{\sqrt{x-\xi}} \tag{3.2.5}$$

where $x_o(y)$ is the leading edge coordinate. When the function α_v is small, the solution of the inviscid problem with trailing edge Kutta condition is a valid solution of the load problem. However, we will see that α_v can become quite large near the trailing edge and at lateral edges that are aligned with the flow. This function can be computed routinely

with the output of a doublet lattice solution of the wing lift problem. It is the 2-D planform Laplacian of the chordwise Abel transform of the doublet strength $\Delta\varphi$.

Prandtl's relations

The differential relationship between shed streamwise vorticity and span loading is well known in classical wing theory. We have already noted that the first two of Equations (3.1.4) are micro versions of Prandtl's early wing theory that follow directly from the Navier Stokes equations. With the representation of vorticity in (3.1.18) we can derive another intermediate load vorticity relationship that illustrates Prandtl's formulas. We define the local circulation components

$$\begin{aligned} \gamma_x &= \int_{-\infty}^{\infty} \omega_x dz & \gamma_y &= \int_{-\infty}^{\infty} \omega_y dz \\ &= \frac{\partial}{\partial y} \int_{-\infty}^{\infty} B\, dz & &= -\frac{\partial}{\partial x} \int_{-\infty}^{\infty} B\, dz \end{aligned} \tag{3.2.6}$$

But

$$\begin{aligned} \int_{-\infty}^{\infty} B\, dz &= -\frac{\sigma}{2\pi} \iint_S d\xi d\eta\, \ell e^{\sigma(x-\xi)} \int_{-\infty}^{\infty} dz \frac{e^{-\sigma R}}{R} \\ &= -\frac{\sigma}{\pi} \iint_S d\xi d\eta\, \ell e^{\sigma(x-\xi)} K_0(\sigma R) \end{aligned} \tag{3.2.7}$$

with

$$R = \left[(x-\xi)^2 + (y-\eta)^2 \right]^{1/2} \tag{3.2.8}$$

Now for $\sigma >> 1$, $K_0(\sigma R)$ has delta function properties with respect to y. Thus

$$K_0(\sigma R) = C\delta(y-\eta) \tag{3.2.9}$$

with

$$\begin{aligned} C &= \int_{-\infty}^{\infty} K_0(\sigma R) dy \\ &= \frac{\pi}{\sigma} e^{-\sigma|x-\xi|} \end{aligned} \tag{3.2.10}$$

and

$$\int_{-\infty}^{\infty} B\, dz = -\iint_S d\xi d\eta\, \ell(\xi,\eta) e^{\sigma((x-\xi)-|x-\xi|)}\delta(y-\eta)$$

$$= -\int_{x_o}^{x} d\xi\, \ell(\xi,y) \qquad (3.2.11)$$

Thus

$$\gamma_x = -\frac{\partial}{\partial y}\int_{x_0}^{x} d\xi\, \ell(\xi,y) \qquad x < x_e$$

$$= -\frac{\partial L}{\partial y} \qquad x > x_e$$

$$\gamma_y = \ell(x,y) \qquad x < x_e$$

$$= 0 \qquad x > x_e \qquad (3.2.12)$$

which are the well-known wing theory relations. For $x > x_e$ (the trailing edge) the spanwise circulation is zero and the streamwise circulation is the negative of the span load.

Drag-due-to-loads

Next we consider the kernel K_E (see (3.1.25)) that appears in the drag-due-to-loads and in the minimum drag problem. It too has delta function properties that we want to exploit. Consider

$$E_1\left(\sigma(R \pm |x|)\right) \equiv C^{\pm}\delta(y)$$

with

$$C^{\pm} = \int_{-\infty}^{\infty} dy\, E_1\left(\sigma(R \pm |x|)\right) \qquad (3.2.13)$$

Integrate by parts to get

$$C^{\pm} = e^{\mp|x|}\int_{-\infty}^{\infty} dy \left(1 \mp \frac{|x|}{R}\right) e^{-\sigma R}$$

$$= 2|x| e^{\mp|x|}\left(K_1(\sigma|x|) \mp K_0(\sigma|x|)\right) \qquad (3.2.14)$$

For $\sigma >> 1$ we obtain the asymptotic results

$$C^+ = 0$$
$$C^- = 4\sqrt{\frac{\pi}{2\sigma}}\,|x| \tag{3.2.15}$$

and

$$K_E(x,y) \equiv 2\sqrt{\frac{\pi}{2\sigma}}\,\sqrt{|x|}\,\delta(y) \tag{3.2.16}$$

Substitute (3.2.16) into (3.1.24) and rewrite after integration by parts as

$$C_D = -\frac{1}{8\pi A}\int_b dy \frac{\partial L}{\partial y}\int_b d\eta\,\frac{\partial L}{\partial \eta}\,\ell n|y-\eta|$$
$$+\frac{1}{4A\sqrt{2\pi\sigma}}\iint_S dxdy\,\ell(x,y)\nabla^2\int_c d\xi\,\ell(\xi,y)\sqrt{|x-\xi|} \tag{3.2.17}$$

where c and b denote integration over the local chord $c(y)$ and total span b. The above result has been derived somewhat formally with little regard for the singular behavoir of $\ell(x,y)$ near free edges. We have already shown with our 2-D analysis that the leading edge singularly leads to an order one contribution to C_D —the leading edge suction or absence thereof. Singularities at the wing tip will also lead to a singular and perhaps order one contribution to C_D. Further analysis will be required to verify or refute this suspision, but the second derivative with respect to y in (3.2.17) is a strong indication that such is the case.

Minimum drag problem

The problem for the minimum drag load distribution can also be reduced by using the above asymptotic approximation for K_E. We write (3.1.31) in the form

$$\frac{1}{4\pi}\frac{\partial^2}{\partial y^2}\cdot\iint_S d\xi d\eta\, F(\xi,\eta)\,\ell n|y-\eta|$$

$$+\frac{1}{4\pi}\nabla^2\cdot\iint_S d\xi d\eta\, F(\xi,\eta)\cdot K_E(x-\xi,y-\eta)=1 \qquad (3.2.18)$$

The second term is the new feature of the viscous theory. Without this term we recover the classical equation for the minimum induced drag span load distribution

$$\frac{1}{4\pi}\frac{\partial^2}{\partial y^2}\int_{-A}^{A} d\eta\, F(\eta)\ell n|y-\eta|=1 \qquad (3.2.19)$$

with the elliptic load solution

$$F(y)=\int_{c(y)} F(x,y)dx=4\sqrt{A^2-y^2} \qquad \|F\|=2\pi A^2$$

and famous formula for induced drag:

$$C_D=\frac{C_L^2}{\pi A}\quad\text{(classical)} \qquad (3.2.20)$$

If the span becomes infinite with uniform chord and we neglect all spanwise derivatives, we recover the 2-D minimum section drag problem that was discussed in Section II.

A plausible method of attacking the combined problem is the following. Since the two integral terms in (3.2.18) are of different asymptotic order we might seek a solution $F(x,y)$ such that each term individually is a constant; i.e.,

$$\frac{1}{4\pi}\frac{\partial^2}{\partial y^2}\int_b d\eta\, F(\eta)\ell n|y-\eta|=C_0$$

$$\frac{1}{2A\sqrt{2\pi}}\nabla^2\int_c d\xi\, F(\xi,y)\sqrt{|x-\xi|}=C_1 \qquad (3.2.21)$$

With

$$C_0 + \frac{C_1}{\sqrt{\sigma}} = 1 \tag{3.2.22}$$

the global span loading $F(y)$ will be elliptic with small $O\left(1/\sqrt{\sigma}\right)$ Reynolds number corrections. Away from the tip region $F(x,y)$ will tend to the 2-D result obtained previously. A more careful numerical analysis of the second of equations (3.2.21) should in principal yield the optimal load distribution near the tip.

We conclude with the remark that the optimal load equation can be expressed compactly as the 2-D Laplacian of a single integral expression; i.e.,

$$\frac{1}{4\pi}\nabla^2 \iint_S d\xi d\eta \, F(\xi,\eta) K_D(x-\xi, y-\eta) = 1 \tag{3.2.23}$$

where K_D is the viscous induced drag kernel (3.1.25). This result follows from the fact that the first term in (3.2.18) is independent of x.

3.3 Example of the separation potential

To conclude our present treatment of the 3-D wing we derive an explicit formula for the high Reynolds number separation potential (3.2.5) and illustrate the result with a numerical example for the rectangular wing. It is convenient to work with the load form of (3.2.5) which we obtain with a single integration by parts. The result is

$$\alpha_v(x,y) = -\frac{1}{\sqrt{2\pi\sigma}}\nabla^2 \int_{x_o}^{x} d\xi \, \ell(\xi,y)\sqrt{x-\xi} \tag{3.3.1}$$

where $\sigma >> 1$. In general we would implement this relation by solving for the inviscid load or doublet strength $\Delta\varphi$ with a trailing edge Kutta condition. Then calculate $\alpha_v(x,y)$ numerically to obtain a map on the surface where separation can be expected—a post processing operation with a doublet lattice solver. Below we assume a general form of the load distribution and derive an analytic expression for α_v.

Consider a load distribution of the form

$$\ell(x,y)=\frac{2}{\pi}\frac{L(y)}{(x_e-x_o)}\sqrt{\frac{x_e-x}{x-x_o}} \tag{3.3.2}$$

where $x_o(y), x_e(y)$ denote the leading and trailing edge of the wing respectively and $L(y)$ is the span load, i.e.,

$$L(y)=\int_{x_o}^{x_e} dx\, \ell(x,y) \tag{3.3.3}$$

Also

$$C_L=\frac{1}{2A}\int_{-A}^{A} L(y)dy \tag{3.3.4}$$

where A is the aspect ratio. Substitute (3.3.2) into (3.3.1) and introduce the change of variables

$$\xi = x_0+2(x_e-x_o)k^2\sin^2\varphi, \qquad 0<\varphi<\pi/2$$
$$k^2=\frac{x-x_o}{x_e-x_o} \tag{3.3.5}$$

We obtain

$$\alpha_v(x,y)=-\frac{4}{3\pi\sqrt{2\pi\sigma}}\nabla^2\left[\tilde{L}(y)J(k)\right] \tag{3.3.6}$$

with

$$\tilde{L}(y)=L(y)(x_e-x_o)^{1/2}$$
$$J(k)=\left(1+k^2\right)E(k)-(1-k^2)K(k) \tag{3.3.7}$$

The elliptic integrals follow from results in Appendix A. The final operation is to reduce the derivatives that are indicated in (3.3.6). We use the known results for derivatives of E and K,

$$E' = \frac{E-K}{k}$$
$$K' = \frac{E}{k(1-k^2)} - \frac{K}{k} \tag{3.3.8}$$

with the following formula for

$$\frac{\partial k}{\partial x} = \frac{1}{2k(x_e - x_o)} \tag{3.3.9}$$

to obtain the following:

$$\frac{\partial J}{\partial x} = \frac{J'(k)}{2(x_e - x_o)k} = \frac{3E}{2(x_e - x_o)}$$
$$\frac{\partial^2 J}{\partial x^2} = \frac{3}{2(x_e - x_o)} \cdot \frac{1}{2(x_e - x_o)k}\left(\frac{E-K}{k}\right)$$
$$= \frac{3(E-K)}{4(x_e - x_o)^2 k^2} \tag{3.3.10}$$

Also

$$\frac{\partial J}{\partial y} = k_y J' = 3k\, k_y\, E$$
$$\frac{\partial^2 J}{\partial y^2} = 3\left(k_y^2 + k\, k_{yy}\right)E + 3k\, k_y^2 \frac{E-K}{k}$$
$$= 3\left(2k_y^2 + k\, k_{yy}\right)E - 3k_y^2 K \tag{3.3.11}$$

where k depends on y through (3.3.5). Introduce the above derivatives into (3.3.6) to obtain

$$\alpha_v(x,y) = \frac{4}{3\pi\sqrt{2\pi\sigma}}\left[\tilde{L}(y)\left(\frac{\partial^2 J}{\partial x^2} + \frac{\partial^2 J}{\partial y^2}\right) + 2\tilde{L}'(y)\frac{\partial J}{\partial y} + \tilde{L}''(y)\cdot J\right]$$

or

$$\alpha_v = -\frac{\tilde{L}(y)}{\pi\sqrt{2\pi\sigma}}\left[\frac{E-K}{(x_e - x_o)(x - x_o)} + 8\left(2k_y^2 + k\, k_{yy}\right)E\right]$$
$$-\frac{8\tilde{L}'(y)}{\pi\sqrt{2\pi\sigma}} \cdot k\, k_y E - \frac{4\tilde{L}''(y)}{3\pi\sqrt{2\pi\sigma}}\left[(1+k^2)E - (1-k^2)K\right] \tag{3.3.12}$$

Rectangular wing

For the special case of a rectangular wing, k is independent of y and,

$$x_o = -1, \qquad x_e = 1, \qquad k^2 = \frac{1+x}{2}, \qquad \tilde{L} = \sqrt{2}L(y) \tag{3.3.13}$$

so that

$$\alpha_v = -\frac{L(y)}{4\pi\sqrt{\pi\sigma}} \cdot \frac{E-K}{k^2} - \frac{4L''(y)}{3\pi\sqrt{\pi\sigma}}\left[(1+k^2)E-(1-k^2)K\right] \tag{3.3.14}$$

Now assume an elliptic span load

$$L(y) = \frac{4}{\pi} C_L \left(1-y^2/A^2\right)^{1/2} \tag{3.3.15}$$

where A is the aspect ratio. Then

$$L'' = -\frac{4C_L}{\pi A^2}\left(1-y^2/A^2\right)^{-3/2} \tag{3.3.16}$$

and

$$\alpha_v = \frac{C_L}{\pi^2\sqrt{\pi\sigma}}\left\{\frac{(K-E)}{k^2}\left(1-y^2/A^2\right)^{1/2} + \frac{16}{3A^2}\left[(1+k^2)E-(1-k^2)K\right]\cdot\left(1-y^2/A^2\right)^{-3/2}\right\} \tag{3.3.17}$$

The first term has a logarithmic singularity along the trailing edge ($k \to 1$) while the second term has a much stronger algebraic singularity at the cut-off rectangular tip—a result of the second y derivative in (3.3.1). The separation potential scales linearly with the lift coefficient and inversely with the square root of the Reynolds number which is typical of most results obtained with the linear viscous theory. The importance of α_v is in its variation over the planform. We have plotted contours of the normalized separation potential

$$S(x,y) = \frac{\sqrt{\sigma}\,\alpha_v}{C_L} \tag{3.3.18}$$

in Figure 3-3 for $A = 4$. Also, we have overlaid contours of the doublet strength

$$\Delta\varphi = -\int_{-1}^{x} \ell(\xi, y)\, d\xi$$
$$= -\frac{4C_L}{\pi^2}\left(1 - y^2/A^2\right)^{1/2}\left(\pi/2 + \sin^{-1} x + \sqrt{1-x^2}\right) \qquad (3.3.19)$$

for a unit lift coefficient. These contours are the vortex field lines which all turn and separate at the trailing edge in accordance with the Kutta condition. The striking feature of the contours of $S(x,y)$ is the singular behavior near the tip. A strong separation zone is indicated that originates at the tip leading edge and spreads inboard along the trailing edge—a physically appealing result.

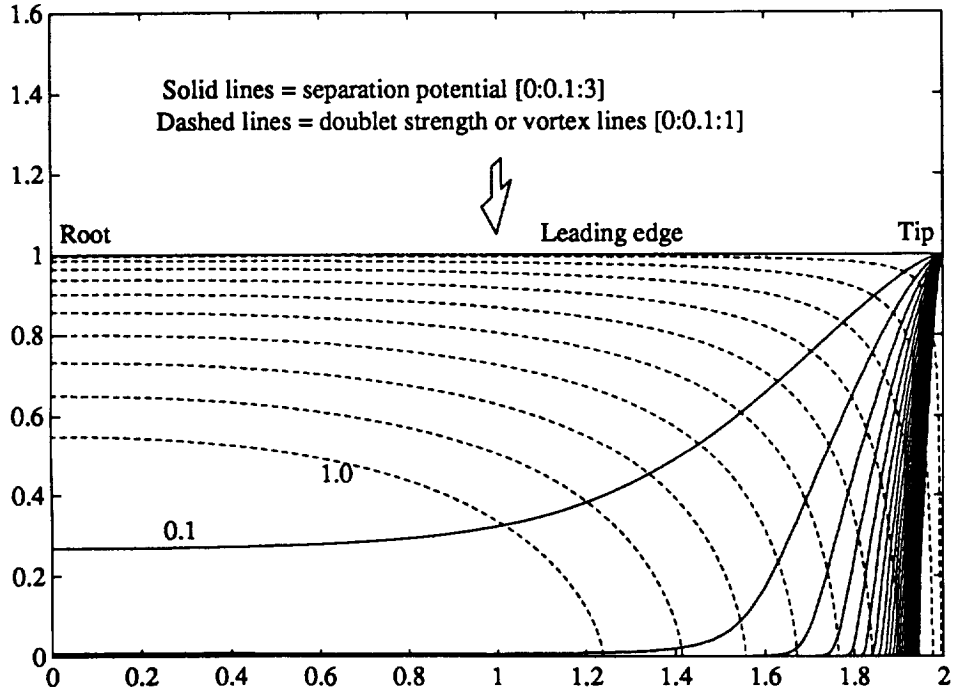

Figure 3-3. Separation potential for a rectangular wing: A = 4.

The tip separation zone is actually indicated in the general formula (3.3.12) if we note that $\tilde{L}''(y)$ is the second span derivative of the product of the span load $\tilde{L}(y)$ times

the square root of the local chord $(x_e\text{-}x_o)^{1/2}$ (see (3.3.7)). This formula also suggests that the tip separation region could be significantly reduced in size by contouring the planform such that the derivatives of $L(y)$ are regular at the tip. For example, assume that L(y) is locally elliptic, i.e.,

$$L(y) = O(1 - y/A)^{1/2} \qquad y \to A \tag{3.3.20}$$

and that

$$x_e - x_0 = O(1 - y/A)^{\upsilon} \tag{3.3.21}$$

Then

$$\tilde{L}(y) = O(1 - y/A)^{\frac{1+\upsilon}{2}} \tag{3.3.22}$$

and the derivatives of L are regular if $\nu = 1$. Thus, a wing tip that tapers smoothly to a point appears to indicate a regular behavior of the separation potential near the tip if our assumption of a local elliptic loading is correct. It is a curious fact that the fins of many marine mammals and fish and many birds have highly pointed wing tips. Also, the wing tips of recent transport aircraft have evolved towards this shape (e.g., the Boeing 757 and 767). For a discussion of skewed and pointed wing tips, see Vijgen, et al. (1987). The small induced drag advantage that these authors report may be secondary compared to the reduction of the separation potential at higher angle of attack.

IV. Conclusions and Recommendations

A unified viscous theory of lift and drag of thin 2-D airfoils and 3-D lifting surfaces has been developed in detail. The theory is *"complete"* in the formal sense of Birkhoff's reversibility paradox stated in Section II but far from complete in terms of the opportunities that it opens up for future research and technical applications. We summarize the main conclusions of our effort and recommend a number of avenues for further research and development.

Summary of conclusions

1. The lift and section drag-due-to-lift of thin 2-D airfoils can be calculated uniquely with the viscous theory developed herein.

2. The high Reynolds number limit of the calculated lift $(c_L = 2\pi\alpha)$ is in agreement with inviscid theory that uses the trailing edge Kutta condition. The high Reynolds number section induced drag limit $(c_D = c_L^2 / 2\pi)$ is in agreement with experimental results. The theory shows conclusively that the section induced drag is due to viscous action at the leading edge.

3. The section induced drag of profiled airfoils is of order $1/\sqrt{R_N}$ where R_N is the Reynolds number based on the leading edge radius. While the scaling appears to be correct (see Henderson and Holmes 1989), the magnitudes are about an order of magnitude smaller than those reported for very thin NACA four digit series foils that operate in turbulent flow. The calculated levels are in closer agreement with experimental values for the *"laminar flow bucket"*. The role of turbulent enstrophy and drag is discussed.

4. The theory of minimum section induced drag is a significant new contribution to the theory of thin airfoils to the Author's knowledge. For the same lift coefficient, the theoretical drag minimum is only about four percent smaller than the drag of a foil with parabolic camber. The slope of the camber shape, however, is much more cusped at the leading and trailing edges.

5. The minimum section induced drag corresponds to a constant value of the section induced drag angle. The product of the load and the induced drag angle yields the local

drag. This result is completely analogous to a constant downwash angle for minimum drag in classical 3-D minimum wing drag theory. Minimum drag results are computed and compared with those for the constant angle of attack and parabolic camber configurations over 7 decades of Reynolds number from Stokes flow to 10,000.

6. The concept of a viscous induced *"separation potential"* is introduced with detailed calculations for constant angle of attack, parabolic camber and an airfoil with trailing edge flap. In the high Reynolds number limit, this new function can be computed with a simple post processing operation on the load or doublet strength output of a standard wing theory code. Nonlinear boundary layer calculations are not required. The three example calculations indicate separation near the trailing edge and hinge line as we would expect. The separation potential is a valuable design tool.

7. The viscous 3-D wing theory is formally complete even though we have not obtained as many numerical examples as we would like - in particular a demonstration of the optimal load distribution for candidate wing planforms.

8. The load/upwash kernel function of the 3-D viscous theory is less singular than its inviscid counterpart. A unique solution of the load equation can be calculated without recourse to a Kutta condition along the trailing edge. In the high Reynolds number limit, the classical inviscid solution with Kutta condition will be obtained - proved by asymptotic analysis.

9. One of the most (if not the most) important results of our work is a 3-D viscous induced drag kernel function (see Figure 3-2). The correlation of the spanwise load gradients in this kernel yields the classical induced drag in the high Reynolds number limit. Furthermore, all of the 2-D section results can be recovered for high aspect ratio wings when the correlation of chordwise load gradients in the kernel dominate the induced drag. The interaction of spanwise and chordwise gradients at the wing tip is a topic that should be given immediate attention with the new theory.

10. The 3-D viscous theory of minimum induced drag yields an equation for the universal minimum drag load distribution both spanwise and chordwise for a given planform. The use of this equation to analyze and synthesize wing tip designs is highly recommended.

11. The concept of a viscous separation potential is extended to 3-D with an explicit high Reynolds number example for a rectangular wing. Separation along the wing tip starting at the leading edge is predicted (see Figure 3-3). Again, the 3-D separation potential can be calculated with the output of a panel code without resorting to boundary layer calculations.

Recommendations

The viscous theory and concepts developed in this report open up a new avenue of thinking about the fundamental *viscous* forces that act on a body in a moving fluid medium;i.e., the lift and the drag. The theory is more than a conceptual exercise in that the fundamental forces can be calculated from viscous first principles without recourse to engineering empiricisms like the Kutta condition or the leading edge suction analogy. At the same time, the theory does not invalidate but rather reinforces the use of these tools at a deeper level. The theory also provides a solid foundation for further investigation of some of the more difficult problems of airfoil and wing theory that involve geometric thickness, finite angle of attack, turbulence and compressibility. The oscillating airfoil and wing and motions that are designed for propulsion are amenable to the type of analysis presented herein. In fact the original motivation for and effort on the viscous thin airfoil problem was to solve the unsteady problem. The unsteady form of the resultant axial force contains the drag discussed herein plus an additional term that represents the work done by the pressure forces. This term can oppose the drag and thus makes it possible to design optimal propulsion configurations. There are many possible avenues of fruitful research. We enumerate a few of the more important ones below.

1. Complete the program for the 3-D wing with extensive numerical examples of optimal minimum drag loading and separation potential for different planform shapes and camber distributions. Place particular emphasis on the analysis and synthesis of wing tip shapes.

2. Include geometric thickness and mean boundary layer displacement thickness in the basic viscous analysis of the 2-D and 3-D thin surface. Compare calculations with the wealth of experimental data - in particular separation data. Quantify, if possible, the concept of separation potential by direct correlation with experimental data.

3. Develop the entire viscous program for small amplitude oscillatory motion of finite thickness foils and wings. Drag and separation potential due to unsteady motion can be calculated.

4. Include compressibility in the viscous formulation. The viscous origin of the fundamental forces should become even more important as speeds become transonic.

5. Develop the minimum drag/maximum thrust analog of the theory to aid in the design of optimal propulsion configurations.

6. Develop a rational theory of drag due to turbulent enstrophy and incorporate it into the section induced drag theory.

References

Abbott, Ira H. and von Doenhoff, Albert E. 1959 *Theory of Wing Sections* Dover Publications, Inc., New York.

Abromowitz, M. and Stegun, I. A. eds. 1964 *Handbook of Mathematical Functions (2nd Printing)* National Bureau of Standards, Washington, D. C.

Batchelor, G. K. 1967 *An Introduction to Fluid Dynamics* Cambridge University Press, p. 227.

Birkhoff, Garrett 1955 *Hydrodynamics - a study in logic fact and similitude* Dover Publications, Inc., New York.

Brown, S. N. and Stewartson, K. J. 1970 *Trailing Edge Stall* Jour. Fluid Mech., **Vol 42**, p. 561.

Carrier, G. F., Krook, M. and Pearson, C. E. 1966 *Functions of a Complex Variable - Theory and Technique* McGraw-Hill, Inc., New York, Ch. 8.

Erdelyi, A. ed. 1954 *Table of Integral Transforms* Bateman Manuscript Project **Vol. 1** McGraw-Hill Book Co., Inc., New York.

Greene, George C. 1988 *Viscous Induced Drag* AIAA Paper No. 88-2550 Presented at the Sixth Applied Aerodynamics Conference, Williamsburg, VA June 6-8. (Also see "An Entropy Method for Drag Minimization." SAE Technical Paper Series 892344 September 1989.)

Groebner, Wolfgang and Hofreiter, Nikolaus 1961 *Unbestimmte und Bestimmte Integrale* Springer-Verlag.

Henderson, William P. and Holmes, Bruce J. 1989 *Induced Drag - Historical Perspective* SAE Aerotech '89 Conference, Anaheim, CA, (September 25-28).

Hoerner, S. F. 1965 *Fluid-Dynamic Drag* Published by the author, Hoerner Fluid Dynamics, P.O. 342, Brick Town, NJ 09723.

Holmes, Bruce J. 1990 *Prospects for Drag Reduction* AIAA Professional Studies Series 1990 *Drag-Prediction and Measurement* Portland, Oregon (August 23-24).

Horne, W.Clifton., Smith, Charles A. and Karamcheti, Krishnamurty 1990 *Some Aeroacoustic and Aerodynamic Applications of the Theory of Nonequilibrium Thermodynamics* AIAA paper 90-3989 (October 22-24).

McLean, J. D. 1990 *Viscous Drag* AIAA Professional Studies Series 1990 *Drag-Prediction and Measurement* Portland, Oregon (August 23-24).

Melnik, R. E. 1978 *Wake Curvature and Trailing Edge Interaction Effects in Viscous Flow Over Airfoils* ATAR Conference, NASA Langley Research Center, Hampton, VA (March 7-9).

Rooney, E. C. 1990 *The Determination of Drag from Flight Tests* AIAA Professional Studies Series 1990 *Drag-Prediction and Measurement* Portland, Oregon (August 23-24).

Shen, S. F. and Crimi, P. 1965 *The Theory for an Oscillating Thin Airfoil as Derived from the Oseen Equations* Jour. Fluid Mech., **Vol. 23**, part 3, pp. 585-609.

Southwell, R. W. and Squire, H. B. 1933 *A Modification of Oseen's Approximate Equations for the Motion in Two Dimensions of a Viscous Incompressible Fluid* Phil. Trans. of Roy. Soc., Series A, **232**, 27.

van der Vooren, J. and Slooff, J. W. 1990 *CFD-Based Drag Prediction; State-of-the-Art, Theory, Prospects* AIAA Professional Studies Series 1990 *Drag-Prediction and Measurement* Portland, Oregon (August 23-24).

Vijgen, P.M.H.W., Van Dam, C.P. and Holmes, B.J. 1987 *Sheared Wing-Tip Aerodynamics: Wind-Tunnel and Computational Investigations of Induced-Drag Reduction* AIAA paper 87-2481 CP, 5th Applied Aerodynamics Conference, Monterey, CA (August 17-19).

Yates, John E. 1990 *Prediction of Drag and Lift - a Viscous/Thermodynamic Approach* AIAA Professional Studies Series 1990 *Drag-Prediction and Measurement* Portland, Oregon (August 23-24).

Yates, John E. and Donaldson, Coleman duP. 1986 *A Fundamental Study of Drag and an Assessment of Conventional Drag-due-to-Lift Reduction Devices* NASA Contractor Report 4004 (September).

Yates, John E. 1986 *The Development and Application of a Unified Viscous Theory of Drag and Lift* ARAP Tech Memo 86-12 (April).

Yates, John E. 1983 *A Research Prospectus on the Viscous Theory of Lift and Related Problems in Aeroacoustics* ARAP Tech. Memo. 83-5 (April).

Yates, John E. 1982 *A Study of Thickness and Viscous Effects in Unsteady Three-Dimensional Lifting Surface Theory* ARAP Report No. 463 prepared for NASA Langley Research Center, Contract No. NAS1-16241 (January).

Yates, John E. 1980 *Viscous Thin Airfoil Theory* ARAP Report No. 413 prepared for Office of Naval Research, Contract No. N00014-77-C-0616 (February). (Also see *Viscous Thin Airfoil Theory and the Kutta Condition* AIAA Paper No. 78-152, January 1978 and *Unsteady Viscous Thin Airfoil Theory* AGARD Report No. 671 January 1979).

Appendix A
2-D Separation Potentials

1. Constant angle of attack (see (2.2.20))

$$\alpha_v(x) = -\frac{1}{2\pi\sqrt{2\pi\sigma}}\frac{\partial}{\partial x}\cdot\int_{-1}^{x}\frac{d\xi}{\sqrt{x-\xi}}\frac{c_L - 2\pi\alpha\xi}{\sqrt{1-\xi^2}} \tag{A.1}$$

Let

$$\xi = -1 + (1+x)\sin^2\phi \qquad 0 < \phi < \pi/2 \tag{A.2}$$

so that

$$\sqrt{(1-\xi^2)(x-\xi)} = \sqrt{2}\frac{1+x}{2}\sin 2\phi\sqrt{1-k^2\sin^2\phi}$$

$$k = \sqrt{\frac{1+x}{2}}, \qquad \frac{d\xi}{\sqrt{(1-\xi^2)(x-\xi)}} = \sqrt{2}\frac{d\phi}{\sqrt{1-k^2\sin^2\phi}} \tag{A.3}$$

Thus

$$\alpha_v(x) = -\frac{1}{2\pi\sqrt{\pi\sigma}}\frac{\partial}{\partial x}\left[(c_L - 2\pi\alpha)K(k) + 4\pi\alpha E(k)\right] \tag{A.4}$$

with

$$E(k) = \int_0^{\pi/2} d\phi\sqrt{1-k^2\sin^2\phi}, \qquad K(k) = \int_0^{\pi/2} d\phi/\sqrt{1-k^2\sin^2\phi} \tag{A.5}$$

With the derivative formulas,

$$E'(k) = (E-K)/k, \qquad K'(k) = \frac{E}{k(1-k^2)} - \frac{K}{k}, \qquad \frac{dk}{dx} = \frac{1}{4k} \tag{A.6}$$

we obtain

$$\alpha_v(x) = -\frac{1}{8\pi\sqrt{\pi\sigma}k^2}\left[(c_L - 2\pi\alpha)(E/(1-k^2) - K) + 4\pi\alpha(E-K)\right] \tag{A.7}$$

2. Parabolic camber (see(2.2.27))

$$\alpha_v = -\frac{c_L}{\pi\sqrt{2\pi\sigma}}\frac{\partial}{\partial x}\cdot\int_{-1}^{x} d\xi\frac{\sqrt{1-\xi^2}}{\sqrt{x-\xi}}$$

$$1-\xi^2 = 2(1-k^2\sin^2\phi)(1+x)\sin^2\phi = 4k^2(1-k^2\sin^2\phi)\sin^2\phi$$

$$\alpha_v = -\frac{c_L}{\pi\sqrt{2\pi\sigma}}\frac{\partial}{\partial x}\int_0^{\pi/2} d\phi\sqrt{2}\cdot 4k^2\sqrt{1-k^2\sin^2\phi}\sin^2\phi$$

$$= -\frac{4c_L}{\pi\sqrt{\pi\sigma}}\frac{\partial}{\partial x}\left[k^2\int_0^{\pi/2} d\phi\sqrt{1-k^2\sin^2\phi}\sin^2\phi\right]$$

$$= -\frac{2c_L}{\pi\sqrt{\pi\sigma}}\int_0^{\pi/2} d\phi\left[\sqrt{1-k^2\sin^2\phi} - \frac{\sin^2\phi}{2\sqrt{1-k^2\sin^2\phi}}\right]\sin^2\phi$$

$$= \frac{c_L}{\pi\sqrt{\pi\sigma}}\left[\int_0^{\pi/2} d\phi\frac{\sin^2\phi}{\sqrt{1-k^2\sin^2\phi}} - 3\int_0^{\pi/2} d\phi\sqrt{1-k^2\sin^2\phi}\sin^2\phi\right]$$

$$= \frac{c_L}{\pi\sqrt{\pi\sigma}}\left[\frac{K-E}{k^2} - 3\vartheta\right] \tag{A.8}$$

with

$$\vartheta = \int_0^{\pi/2} d\phi\sqrt{1-k^2\sin^2\phi}\sin^2\phi \tag{A.9}$$

Let $m = k^2$ and write

$$\vartheta = E - \int_0^{\pi/2} d\phi\sqrt{1-m\sin^2\phi}\cos^2\phi \tag{A.10}$$

Now integrate by parts to get

$$\vartheta = E - \int_0^{\pi/2} d\phi \left[\sqrt{1 - m\sin^2\phi}\,\sin^2\phi + \frac{m\sin^2\phi\cos^2\phi}{\sqrt{1 - m\sin^2\phi}} \right]$$

$$= E - \vartheta - \int_0^{\pi/2} d\phi \frac{\cos^2\phi(m\sin^2\phi - 1 + 1)}{\sqrt{1 - m\sin^2\phi}}$$

$$= E - \vartheta - (K - E) + \int_0^{\pi/2} d\phi \sin^2\phi \left[\frac{1}{\sqrt{1 - m\sin^2\phi}} - \sqrt{1 - m\sin^2\phi} \right]$$

$$= E - 2\vartheta - K + E + \frac{1}{m} \int_0^{\pi/2} d\phi \frac{m\sin^2\phi - 1 + 1}{\sqrt{1 - m\sin^2\phi}}$$

$$= 2E - 2\vartheta - K + \frac{K - E}{m}$$

or

$$\vartheta = [(1/m - 1)K + (2 - 1/m)E]/3 \tag{A.11}$$

and

$$\alpha_v = \frac{c_L}{\pi\sqrt{\pi\sigma}}(K - 2E) \tag{A.12}$$

3. Foil with flap

Consider the solution of the inviscid load equation

$$\frac{1}{\pi}\int_{-1}^{1} d\xi \frac{\ell(\xi)}{x-\xi} = 2\alpha(x) \tag{A.13}$$

with

$$\alpha(x) = \beta H(x - x_o) \tag{A.14}$$

where β is the flap angle and x_o is the hinge line. The solution of the load problem with trailing edge Kutta condition is outlined below. The numerical algorithm for evaluating the separation potential follows.

Load distribution

The general solution of (A.13) for any function $\alpha(x)$ is

$$\ell(x) = \frac{1}{\pi\sqrt{1-x^2}}\left[\; c_L - 2\int_{-1}^{1} d\xi \frac{\sqrt{1-\xi^2}\,\alpha(\xi)}{x-\xi}\right] \tag{A.15}$$

For α given by (A.14) we evaluate

$$\bar{\ell}(x) = \; 2\beta\int_{x_o}^{1} d\xi \frac{\sqrt{1-\xi^2}}{x-\xi}$$

$$= \; 2\beta(1-x^2)\int_{x_o}^{1} \frac{d\xi}{\sqrt{1-\xi^2}(x-\xi)} + 2\beta\int_{x_o}^{1} d\xi \frac{x+\xi}{\sqrt{1-\xi^2}}$$

$$= 2\beta\left[(1-x^2)Z + x\cos^{-1} x_o + \sqrt{1-x_o^2}\right] \tag{A.16}$$

with

$$Z = \int_{x_o}^{1} \frac{d\xi}{\sqrt{1-\xi^2}(x-\xi)}$$

$$= \int_{0}^{\cos^{-1} x_o} \frac{d\theta}{x-\cos\theta} \qquad x < x_o$$

$$= -\int_{\cos^{-1} x_o}^{\pi} \frac{d\theta}{x-\cos\theta} \qquad x > x_o \tag{A.17}$$

Use the known integral (Groebner and Hofreiter, Unbestimmte Integrale (1961), p.122)

$$\int \frac{d\theta}{x-\cos\theta} = \frac{1}{\sqrt{1-x^2}} \log C\left[\frac{-1+x\cos\theta+\sqrt{1-x^2}\sin\theta}{x-\cos\theta}\right] \tag{A.18}$$

to get

$$Z = \frac{1}{\sqrt{1-x^2}} \log\left|\frac{-1+xx_o+\sqrt{1-x_o^2}\sqrt{1-x^2}}{x-x_o}\right| \tag{A.19}$$

and

$$\ell(x) = \frac{1}{\pi\sqrt{1-x^2}}\left[c_{_L} - 2\beta(x\cos^{-1} x_o + \sqrt{1-x_o^2}\right.$$

$$\left. -2\beta\sqrt{1-x^2}\log\left|\frac{1-xx_o-\sqrt{1-x_o^2}\sqrt{1-x^2}}{x-x_o}\right|\right] \tag{A.20}$$

To satisfy the Kutta condition at x = 1, we require

$$2\beta = \frac{c_L}{\cos^{-1} x_o + \sqrt{1-x_o^2}} \tag{A.21}$$

and

$$\ell(x) = \frac{c_L}{\pi(\cos^{-1} x_o + \sqrt{1-x_o^2})}\left[\cos^{-1} x_o\sqrt{\frac{1-x}{1+x}} - \log\left|\frac{1-xx_o-\sqrt{1-x_o^2}\sqrt{1-x^2}}{x-x_o}\right|\right] \tag{A.22}$$

Separation potential

The separation potential is given by

$$\alpha_v = -\frac{\partial f_v}{\partial x}$$

with

$$f_v = \frac{1}{2\sqrt{2\pi\sigma}} \int_{-1}^{x} d\xi \frac{\ell(\xi)}{\sqrt{x-\xi}} \tag{A.23}$$

We interpret $f_v(x)$ as the viscous induced camber. Since the load distribution has a log singularity at $x = x_o$, we split the integral (A.23) into two parts $x < x_o$ and $x > x_o$. Also, we observe that the first term in (A.22) is the load distribution for constant angle of attack. Thus, we can use the results (A.4) and (A.7) with $c_L = 2\pi\alpha$ to get,

$$f_{v_o} = \frac{c_L}{\pi\sqrt{\pi\sigma}} E(k)$$

$$\alpha_{v_o} = \frac{c_L}{4\pi\sqrt{\pi\sigma}} \cdot \frac{K-E}{k^2} \tag{A.24}$$

with

$$k^2 = \frac{1+x}{2} \tag{A.25}$$

and

$$f_v = \frac{\cos^{-1} \cdot f_{v_o} - \overline{f}_v}{\cos^{-1} x_o + \sqrt{1-x_o^2}}$$

$$\alpha_v = \frac{\cos^{-1} x_o \cdot \alpha_{v_o} + \partial \overline{f}_v / \partial x}{\cos^{-1} x_o + \sqrt{1-x_o^2}} \tag{A.26}$$

with

$$\bar{f}_v = \frac{c_L}{2\sqrt{2\pi\sigma}} \int_{-1}^{x} d\xi \frac{\bar{\ell}(\xi)}{\sqrt{x-\xi}} \qquad x < x_o$$

$$= \frac{c_L}{2\sqrt{2\pi\sigma}} \left[\int_{-1}^{x_o} d\xi \frac{\bar{\ell}(\xi)}{\sqrt{x-\xi}} + \int_{x_o}^{x} d\xi \frac{\bar{\ell}(\xi)}{\sqrt{x-\xi}} \right] \qquad x > x_o \tag{A.27}$$

and

$$\bar{\ell}(x) = \log \left| \frac{1 - x x_o - \sqrt{1-x_o^2}\sqrt{1-x^2}}{x - x_o} \right| \tag{A.28}$$

For each of the three integrals (a to b) in (A.27), we set

$$\xi = a + (b-a)\sin^2\phi, \qquad d\xi = 2(b-a)\sin\phi\cos\phi d\phi \tag{A.29}$$

The result is

$$\bar{f}_v = c_L \sqrt{\frac{1+x}{2\pi\sigma}} \cdot \int_0^{\pi/2} d\phi \sin\phi \cdot \bar{\ell}(-1 + (1+x)\sin^2\phi) \qquad -1 < x < x_o$$

$$= c_L \sqrt{\frac{1+x_o}{2\pi\sigma}} \cdot \int_0^{\pi/2} d\phi \frac{\sin\phi\cos\phi \cdot \ell(-1 + (1+x_o)\sin^2\phi)}{\sqrt{\frac{1+x}{1+x_o} - \sin^2\phi}}$$

$$+ c_L \sqrt{\frac{x-x_o}{2\pi\sigma}} \cdot \int_0^{\pi/2} d\phi \sin\phi \cdot \ell(x_o + (x-x_o)\sin^2\phi) \qquad x_o < x < 1 \tag{A.30}$$

The above formula is used in Section 2.3 to calculate the viscous induced camber for the 2-D airfoil with flap. The separation potential is calculated by numerical differentiation in each interior analytic region. The numerical algorithm was also checked against the analytic results for the constant angle of attack and parabolic camber cases.

Appendix B
3D Viscous drag-due-to-lift

We derive a 3-D formula for viscous drag-due-to-lift in this appendix starting with (3.1.6) of the main text with the auxiliary definitions (3.1.18):

$$C_D = \frac{1}{4A\sigma}\int_V dV(\omega_x^2+\omega_y^2) \tag{B.1}$$

with

$$\omega_x = \frac{\partial B}{\partial y}, \qquad \omega_y = -\frac{\partial B}{\partial x}$$

$$B = -\frac{\sigma}{2\pi}\iint_S d\xi d\eta \cdot \ell(\xi,\eta)\frac{\exp((\sigma(x-\xi-R))}{R}$$

$$R = \left[(x-\xi)^2+(y-\eta)^2+z^2\right]^{1/2} \tag{B.2}$$

Substitute (B.2) into (B.1), take the x and y derivatives inside the integral over S and interchange the order of integration with respect to V and S. We obtain

$$C_D = -\frac{1}{8\pi A}\left[\iint_S d\xi d\eta \frac{\partial \ell}{\partial \xi}\iint_S d\xi' d\eta' \frac{\partial \ell}{\partial \xi'}\cdot \mathrm{X}(|\xi-\xi'|,|\eta-\eta'|)\right.$$

$$\left. +\iint_S d\xi d\eta \frac{\partial \ell}{\partial \eta}\iint_S d\xi' d\eta' \frac{\partial \ell}{\partial \eta'}\mathrm{X}(|\xi-\xi'|,|\eta-\eta'|)\right] \tag{B.3}$$

with

$$\mathrm{X}(\xi,\eta) = -\frac{\sigma}{2\pi}\int_V dxdydz \cdot \exp((\sigma(2x-\xi))\cdot\frac{\exp(-\sigma(R-R'))}{RR'}, \qquad \xi>0 \tag{B.4}$$

where R' is given by (B.2) with $\xi=\eta=0$.

We evaluate $\mathrm{X}(\xi,\eta)$ for the space [V: x<L] where L is some large number that we eventually take to infinity. This step is essential since the integral is improper in the far wake. Write

$$X(\xi,\eta) = -\frac{\sigma}{2\pi}\int_{-\infty}^{L} dx \exp(\sigma(2x-\xi))\cdot I \tag{B.5}$$

with

$$I = \iint_{-\infty} dydz \frac{\exp(-\sigma(R+R'))}{RR'} \tag{B.6}$$

Then use the double Fourier transform to obtain the Parseval relation

$$I = \frac{1}{(2\pi)^2}\iint_{-\infty} d\alpha d\beta e^{i\alpha\eta}\overline{F}^{*}(x-\xi,\alpha,\beta)\overline{F}(x,\alpha,\beta) \tag{B.7}$$

with

$$\overline{F}(x,\alpha,\beta) = \iint_{-\infty} dydz \exp(-i(\alpha y+\beta z))F(x,y,z) \tag{B.8}$$

and

$$F(x,y,z) = \frac{\exp(-\sigma(x^2+y^2+z^2)^{1/2})}{(x^2+y^2+z^2)^{1/2}} \tag{B.9}$$

The asterisk denotes the complex conjugate in (B.7). Next we evaluate (B.8) using standard Fourier cosine transforms:

$$\overline{F}(x,\alpha,\beta) = 4\int_{0}^{\infty} dy \cos\alpha y\cdot\int_{0}^{\infty} dz \cos\beta z\cdot\frac{\exp(-\sigma(x^2+y^2+z^2)^{1/2})}{(x^2+y^2+z^2)^{1/2}} \tag{B.10}$$

or

$$\overline{F}(x,\alpha,\beta) = 4\int_{0}^{\infty} dy \cos\alpha y\cdot K_0\left[(\beta^2+\sigma^2)^{1/2}(x^2+y^2)^{1/2}\right]$$

$$= 2\pi\frac{\exp(-\lambda|x|)}{\lambda} \tag{B.11}$$

with

$$\lambda = (\alpha^2+\beta^2+\sigma^2)^{1/2} \tag{B.12}$$

so that

$$I = \int\int_{-\infty}^{\infty} d\alpha d\beta e^{i\alpha\eta} \cdot \frac{\exp(-\lambda(|x-\xi|+|x|))}{\lambda^2}$$

$$= 4\int_0^{\infty}\int_0^{\infty} d\alpha d\beta \cos\alpha|\eta| \frac{e^{-\lambda\varsigma}}{\lambda^2} \tag{B.13}$$

with

$$\varsigma = |x-\xi|+|x| \geq 0 \tag{B.14}$$

Again evaluate (B.13) using Fourier transforms. Consider

$$f = \int_0^{\infty} d\beta \frac{e^{-\lambda\varsigma}}{\lambda^2}$$

$$\frac{\partial f}{\partial \varsigma} = -\int_0^{\infty} d\beta \frac{e^{-\lambda\varsigma}}{\lambda} = -K_0(\varsigma(\alpha^2+\sigma^2)^{1/2}) \tag{B.15}$$

and

$$f = \int_{\varsigma}^{\infty} d\varsigma K_0(\varsigma(\alpha^2+\sigma^2)^{1/2}) \tag{B.16}$$

Then

$$I = 4\int_0^{\infty} d\alpha \cos\alpha|\eta| \cdot \int_{\varsigma}^{\infty} dt K_0(t(\alpha^2+\sigma^2)^{1/2})$$

$$= 2\pi\int_{\varsigma}^{\infty} dt \frac{\exp(-\sigma(t^2+\eta^2)^{1/2})}{(t^2+\eta^2)^{1/2}} \tag{B.17}$$

and with (B.5) we get

$$X(\xi,\eta) = -\sigma\int_{-\infty}^{L} dx e^{\sigma(2x-\xi)} \cdot \int_{|x-\xi|+|x|}^{\infty} dt \frac{\exp(-\sigma(t^2+\eta^2)^{1/2})}{(t^2+\eta^2)^{1/2}} \tag{B.18}$$

Integrate (B.18) by parts to obtain

$$X = -\frac{1}{2}\int_{-\infty}^{L} dx \exp(\sigma(2x-\xi)) \cdot \frac{\exp(-\sigma(\varsigma^2+\eta^2)^{1/2})}{(\varsigma^2+\eta^2)^{1/2}} (sgn(x-\xi)+sgn\,x) \qquad \text{(B.19)}$$

with

$$\varsigma = |x-\xi| + |x|, \qquad \xi > 0 \qquad \text{(B.20)}$$

Note that

$$\begin{aligned} sgn(x-\xi)+sgn\,x &= -2 \quad for \quad x<0<\xi<L \\ &= 0 \quad for \quad 0<x<\xi<L \\ &= 2 \quad for \quad 0<\xi<x<L \end{aligned} \qquad \text{(B.21)}$$

and

$$X = \int_{-\infty}^{0} + \int_{\xi}^{L} dx \frac{\exp\{\sigma[\varsigma - (\varsigma^2+\eta^2)^{1/2}]\}}{(\varsigma^2+\eta^2)^{1/2}}, \qquad \xi > 0 \qquad \text{(B.22)}$$

with

$$\varsigma = 2x - \xi \qquad \text{(B.23)}$$

a slight change of notation. Now let

$$t = \sigma[(\varsigma^2+\eta^2)^{1/2} - \varsigma]$$

$$\frac{dt}{t} = -\frac{d\varsigma}{(\varsigma^2+\eta^2)^{1/2}} \qquad dx = \frac{d\varsigma}{2} \qquad \text{(B.24)}$$

so that

$$X = -\frac{1}{2}E_1(t(L)) + \frac{1}{2}E_1(\sigma[(\xi^2+\eta^2)^{1/2} + |\xi|]) + \frac{1}{2}E_1(\sigma[(\xi^2+\eta^2)^{1/2} - |\xi|]) \qquad \text{(B.25)}$$

with the exponential integral,

$$E_1(z) = \int_{z}^{\infty} dt \frac{e^{-t}}{t} \qquad \text{(B.26)}$$

For very large L

$$t(L) = \sigma[(2L-\xi)^2 + \eta^2)^{1/2} - (2L-\xi)]$$

$$\cong \sigma\left[(2L-\xi)\left(1+\frac{\eta^2}{2(2L-\xi)^2}+\ldots\right)-(2L-\xi)\right]$$

$$\cong \frac{\sigma\eta^2}{4L} \tag{B.27}$$

For $L >> \sigma\eta^2 / 4$ we obtain

$$E_1(t(L)) \cong -2\ln|\eta| + + \ln(L) + \text{constant} \tag{B.28}$$

But neither the constant nor ln(L) which is really ln(x) contributes to the drag coefficient in (B.3). Thus we can write

$$\mathrm{X} = \ln|\eta| + K_E \tag{B.29}$$

with

$$K_E(\xi,\eta) = \frac{1}{2}[E_1(\sigma(R-|\xi|)) + E_1(\sigma(R+|\xi|))] \tag{B.30}$$

and

$$R = (\xi^2 + \eta^2)^{1/2} \tag{B.31}$$

Finally, we observe that $\ln|\eta|$ is an irrelevant constant in the first integral of (B.3). Thus, with the change of notation $(\xi, \xi') \rightarrow (x, \xi)$ and $(\eta, \eta') \rightarrow (y, \eta)$ we obtain the final expression for the 3-D viscous induced drag coefficient:

$$C_D = -\frac{1}{8\pi A}\iint_S dxdy\frac{\partial \ell}{\partial y}\cdot\iint_S d\xi d\eta\frac{\partial \ell}{\partial \eta}\cdot K_D(x-\xi, y-\eta)$$

$$-\frac{1}{8\pi A}\iint_S dxdy\frac{\partial \ell}{\partial x}\cdot\iint_S d\xi d\eta\frac{\partial \ell}{\partial \xi}\cdot K_D(x-\xi, y-\eta) \tag{B.32}$$

with

$$K_D(x, y) = \ln|y| + \frac{1}{2}\{E_1[\sigma(R-|x|)] + E_1[\sigma(R+|x|)]\} \tag{B.33}$$

A full discussion of this important result may be found in Section 3.2 of the main text.

NASA
National Aeronautics and Space Administration

Report Documentation Page

1. Report No.	2. Government Accession No.	3. Recipient's Catalog No.
NASA CR-4414		

4. Title and Subtitle

A Unified Viscous Theory of Lift and Drag of 2-D Thin Airfoils and 3-D Thin Wings

5. Report Date

December 1991

6. Performing Organization Code

7. Author(s)

John E. Yates

8. Performing Organization Report No.

10. Work Unit No.

505-59-54-01

9. Performing Organization Name and Address

A.R.A.P. Group, California Research & Technology Division
Titan Corporation
50 Washington Road, P. O. Box 2229
Princeton, NJ 08543-2229

11. Contract or Grant No.

L-74809C

12. Sponsoring Agency Name and Address

National Aeronautics and Space Administration
Langley Research Center
Hampton, VA 23665-5225

13. Type of Report and Period Covered

Contractor Report

14. Sponsoring Agency Code

15. Supplementary Notes

Langley Technical Monitor: Lawrence E. Putnam

16. Abstract

A unified viscous theory of 2-D thin airfoils and 3-D thin wings is developed with numerical examples. The viscous theory of the load distribution is unique and tends to the classical inviscid result with Kutta condition in the high Reynolds number limit. A new theory of 2-D section induced drag is introduced with specific applications to three cases of interest: 1) constant angle of attack, 2) parabolic camber, and 3) a flapped airfoil. The first case is also extended to a profiled leading-edge foil. The well-known drag due to absence of leading-edge suction is derived from the viscous theory. It is independent of Reynolds number for zero thickness and varies inversely with the square root of the Reynolds number based on the leading-edge radius for profiled sections. The role of turbulence in the section induced drag problem is discussed. A theory of minimum section induced drag is derived and applied. Two new concepts, the viscous induced drag angle and the viscous induced separation potential are introduced. The separation potential is calculated for three 2-D cases and for a 3-D rectangular wing. The potential is calculated with input from a standard doublet lattice wing code without recourse to any boundary-layer calculations. Separation is indicated in regions where it is observed experimentally. The classical induced drag is recovered in the 3-D high Reynolds number limit with an additional contribution that is Reynolds number dependent. The 3-D viscous theory of minimum induced drag yields an equation for the optimal spanwise and chordwise load distribution.

17. Key Words (Suggested by Author(s))	18. Distribution Statement
Lift and Drag Reynolds number Unified Viscous Theory 2-D Thin Airfoils 3-D Thin Airfoils	Unclassified - Unlimited Subject Category 02

19. Security Classif. (of this report)	20. Security Classif. (of this page)	21. No. of pages	22. Price
Unclassified	Unclassified	100	A05

NASA FORM 1626 OCT 86

For sale by the National Technical Information Service, Springfield, Virginia 22161-2171 NASA-Langley, 1991